AFRL-PR-WP-TR-2003-2074

MINIATURE HEAT PIPE DEVICES FOR GAS TURBINE ENGINE APPLICATIONS

Yiding Cao

Department of Mechanical Engineering
Florida International Institute
Miami, FL 33199

DECEMBER 2002

Final Report for 15 March 1999 – 15 December 2002

Approved for public release; distribution is unlimited.

PROPULSION DIRECTORATE
AIR FORCE RESEARCH LABORATORY
AIR FORCE MATERIEL COMMAND
WRIGHT-PATTERSON AIR FORCE BASE, OH 45433-7251

NOTICE

USING GOVERNMENT DRAWINGS, SPECIFICATIONS, OR OTHER DATA INCLUDED IN THIS DOCUMENT FOR ANY PURPOSE OTHER THAN GOVERNMENT PROCUREMENT DOES NOT IN ANY WAY OBLIGATE THE US GOVERNMENT. THE FACT THAT THE GOVERNMENT FORMULATED OR SUPPLIED THE DRAWINGS, SPECIFICATIONS, OR OTHER DATA DOES NOT LICENSE THE HOLDER OR ANY OTHER PERSON OR CORPORATION; OR CONVEY ANY RIGHTS OR PERMISSION TO MANUFACTURE, USE, OR SELL ANY PATENTED INVENTION THAT MAY RELATE TO THEM.

THIS REPORT HAS BEEN REVIEWED BY THE OFFICE OF PUBLIC AFFAIRS (ASC/PA) AND IS RELEASABLE TO THE NATIONAL TECHNICAL INFORMATION SERVICE (NTIS). AT NTIS, IT WILL BE AVAILABLE TO THE GENERAL PUBLIC, INCLUDING FOREIGN NATIONS.

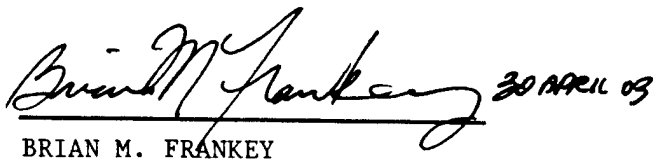

BRIAN M. FRANKEY
Turbine Branch
Turbine Engine Division
Propulsion Directorate

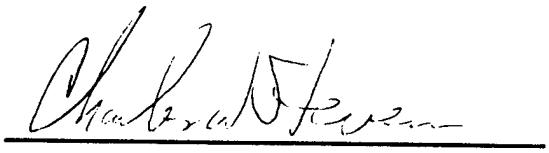

CHARLES W. STEVENS
Chief, Turbine Branch
Turbine Engine Division
Propulsion Directorate

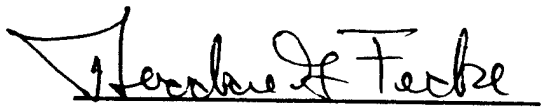

THEODORE G. FECKE
Chief Engineer
Turbine Engine Division
Propulsion Directorate

Do not return copies of this report unless contractual obligations or notice on a specific document requires its return.

REPORT DOCUMENTATION PAGE

Form Approved
OMB No. 0704-0188

1. REPORT DATE *(DD-MM-YY)*	2. REPORT TYPE	3. DATES COVERED *(From - To)*
December 2002	Final	03/15/1999 – 12/15/2002

4. TITLE AND SUBTITLE
MINIATURE HEAT PIPE DEVICES FOR GAS TURBINE ENGINE APPLICATIONS

5a. CONTRACT NUMBER
F33615-99-C-2906

5b. GRANT NUMBER

5c. PROGRAM ELEMENT NUMBER
62203F

6. AUTHOR(S)
Yiding Cao

5d. PROJECT NUMBER
3066

5e. TASK NUMBER
HB

5f. WORK UNIT NUMBER
CU

7. PERFORMING ORGANIZATION NAME(S) AND ADDRESS(ES)
Department of Mechanical Engineering
Florida International Institute
Miami, FL 33199

8. PERFORMING ORGANIZATION REPORT NUMBER

9. SPONSORING/MONITORING AGENCY NAME(S) AND ADDRESS(ES)
Propulsion Directorate
Air Force Research Laboratory
Air Force Materiel Command
Wright-Patterson Air Force Base, OH 45433-7251

10. SPONSORING/MONITORING AGENCY ACRONYM(S)
AFRL/PRTT

11. SPONSORING/MONITORING AGENCY REPORT NUMBER(S)
AFRL-PR-WP-TR-2003-2074

12. DISTRIBUTION/AVAILABILITY STATEMENT
Approved for public release; distribution is unlimited.

13. SUPPLEMENTARY NOTES

14. ABSTRACT

Material temperature limitations impose an upper limit on the amount of work able to be extracted from a turbine. Cooling technologies allow turbine material to remain below upper temperature limitations while allowing for hotter combustor exit temperatures. Increased cooling effectiveness can also decrease cost by decreasing material temperature requirements and allowing for the use of more readily available and manufacturable materials. Miniature heat pipes effectively reduce the maximum and average temperature at the outer rim of a turbine disk. The radial rotating miniature heat pipes employ the centripetal force of the rotating disk to accelerate the condensed cool fluid at the center to the outside and convect the less dense heated fluid from the outside to the inside. The cooling effectiveness of radial rotating heat pipe was investigated through tests and numerical simulations. The test rig and simulation model were simplified models of what is experienced in a rotating turbine disk. Defining parameters were varied. The tests proved that the radial rotating high-temperature heat pipes had a high effective thermal conductance, which is 60 – 100 times greater than the thermal conductivity of copper.

15. SUBJECT TERMS
turbine disk cooling heat pipes

16. SECURITY CLASSIFICATION OF:			17. LIMITATION OF ABSTRACT:	18. NUMBER OF PAGES	19a. NAME OF RESPONSIBLE PERSON (Monitor)
a. REPORT	b. ABSTRACT	c. THIS PAGE			Brian Frankey
Unclassified	Unclassified	Unclassified	SAR	98	19b. TELEPHONE NUMBER *(Include Area Code)* (937) 255-6768

Table of Contents

ABSTRACT

A radially rotating miniature high-temperature heat pipe employs centrifugal force to return the condensate from the condenser section to the evaporator section. The heat pipe has a simple structure, very high effective thermal conductance and large heat transfer capacity, and can work in hostile high-temperature environments. A direct application of the miniature heat pipe is to cool the turbine disk of an advanced aircraft gas turbine engine, where the excessively high temperature at disk rims is a serious problem that needs to be overcome.

In this research project, a high-speed rotating test apparatus and data acquisition system for radially rotating miniature heat pipes are established. Extensive experimental tests on two high-temperature heat pipes with different dimensions are performed, and various effects of the important parameters on the performance characteristics of the heat pipes are investigated. The ranges of the important parameters covered in the experiments are: $470 \le \omega^2 \overline{Z}_a / g \le 1881$; 47 W $\le Q \le$ 325 W; d_i=1.5 and 2 mm; and 1.05×10^{-3} m^3/s $\le W \le 13.4 \times 10^{-3}$ m^3/s. The experimental data prove that the radially rotating miniature high-temperature heat pipe has a high effective thermal conductance, which is 60-100 times higher than the thermal conductivity of copper (including the shell effect), and a large heat transfer capacity that is more than 300 W. Therefore, the heat pipe appears to be feasible for cooling high-temperature gas turbine components.

After the heat pipes are demonstrated, extensive numerical simulations are undertaken for heat-pipe-cooled turbine disks. Thermal performances are compared for the disks with and without incorporating the heat pipe at different heating and cooling

conditions. The numerical results indicate that radially rotating heat pipes can significantly reduce the maximum and average temperatures at the disk rim and dovetail surface under a high heat flux working condition. In general, the maximum and average temperatures at the disk rim and dovetail surface could be reduced by up to 250 K and 150 K, respectively, compared to those of the disk without the heat pipe. As a result, a disk incorporating radially rotating heat pipes could alleviate temperature-related problems and allow a gas turbine to work at a higher temperature.

To obtained a closed-form solution for the design of a turbine disk, temperature distributions in a rotating disk subject to an intense heat input at the disk rim are analytically studied. A closed-form solution is derived based on the disk having a homogenous thermal conductivity. The analytical solution illustrates that the temperature distribution in the disk is a function of heat flux, effective thermal conductance of the disk, heat transfer coefficients at the disk lateral surfaces, and disk geometry. The closed-form solution is then modified for a disk with a discrete heat pipe arrangement along the circumference. To obtain an appropriate modification factor of the closed-form solution, extensive numerical simulation is undertaken and the results are summarized through a correlation. The modified closed-form solution thus obtained predicts the performance of the disk having a discrete heat pipe arrangement with a high accuracy. Compared to the disk without incorporating the heat pipe, a disk incorporating radially rotating heat pipes would have an enhanced thermal dissipation capacity, which results in a much lower temperature at the disk rim due to a substantially increased effective thermal conductance near the disk rim.

After the cooling effect of the heat pipe is demonstrated, a disk/blade assembly incorporating the heat pipe is numerically simulated. This numerical investigation is based on a comparison between a proposed disk/blade assembly incorporating radially heat pipes and a conventional disk/blade assembly without the heat pipes under the same heating and cooling conditions. The numerical investigation illustrates that the turbine disk cooling technique incorporating radially rotating heat pipes is feasible. The temperature distribution at the proposed disk rim can be reduced effectively in comparison with that of a conventional disk without heat pipes. For a proposed disk-blade assembly employing miniature heat pipes, the temperature at the disk rim can be decreased by more that 100 degree, but the average temperature at the blade airfoil surface can be reduced by only about 10 degree. One of the possible causes could be that the heat pipe is not used in the turbine blade. However, it is unclear at this point that the use of the heat pipe in the turbine blade would significantly reduce the blade temperature in conjunction with the use of the heat pipe in the turbine disk. Cooling air properties also play an important role in the disk cooling technology. A lower cooling air temperature will result in a better cooling effect on the disk and blade. In addition, both the heat pipe length and diameter have a very important effect on the turbine disk cooling. Under the permission of material strength, a longer or a larger heat pipe will produce a lower temperature distribution at the disk rim.

1. BACKGROUND

Temperature limitations are one of the most crucial limiting factors to the efficiency of military gas turbine engines. An increased turbine inlet temperature decreases both specific fuel and air consumption while increasing efficiency. This desire for a higher turbine inlet temperature, however, is often in conflict with materials available to withstand this high temperature. Like turbine blades and nozzle guide vanes of an aero-engine, turbine disks are cooled by compressed air that is bled from the compressor. However, as the turbine is exposed to an increasingly high temperature, the disk rim temperature may also reach an unbearably high level. For example, the local disk rim temperature of a high-pressure turbine in an advanced development engine, under the Air Force program of the Integrated High Performance Turbine Engine Technology (HIPSTER), may approach 1000 °C, which could exceed the long term creep limitation of the present disk materials. A literature survey regarding the turbine disk cooling reveals that although the average air-cooling heat transfer coefficient is generally high, the local heat-transfer coefficient at the disk rim is low. Jet cooling could be used to enhance heat transfer at the rim, but its implementation is costly (Metzger, 1970; Metzger and Grochowsky, 1977; Metzger et al., 1979; Owen, 1988, 1992). For miniature military aircraft such as miniature helicopters and miniature surveillance aircraft, it can be envisioned that the temperature limit associated with the aircraft engines would become more severe because of their small size. When the engine size is reduced, the heat transfer surface area available for the cooling purpose is diminished. As a result, the conventional air cooling method would have difficulties to adequately cool engine components and maintain them at a reasonably low temperature. It is clear from

the above discussion that to further advance the state-of-the-art of military aircraft gas turbine engines, a new cooling technique is needed.

For many other advanced military rotating electrical machines, such as alternators, generators, actuators-motors, and integral stators/generators, the severity of the temperature related problems are being realized. These machines are being designed and built using advanced technologies that focus on shrinking the size and increasing the power-to-weight ratio. Of particular interest are the permanent magnet rotor technology and the switched reluctance rotor technology that are the improvement over the existing wound-rotor technology (Ponnappan et al., 1997). Some of these machines are actually in the miniature range. The heat transfer and cooling of the rotors in these machines are critical issues that have to be addressed for a successful operation of these machines. Many of these rotating machines would work under extreme conditions such as high speed, high windage loss, and high-g loading that would affect the thermal condition and control of the rotor in an electrical machine. For example, power densities of 2-5 kW/lb and rotor tip velocity up to 1030 ft/s may be encountered and nearly 20% of the rated power capacity may be dissipated as waste heat within the machine. In all these cases, the rotor or shaft must be adequately cooled. Because of these extreme working conditions and size constraints of the miniature rotating machines, advanced cooling methods and devices must be employed.

For the gas turbine disk discussed earlier, it is believed that one of the major causes of the high disk rim temperature is the low thermal conductivity associated with the turbine disk material. Based on this understanding, a turbine disk that incorporates radially rotating heat pipes has been proposed. The concept of cooling the disk by

employing the heat pipe cooling technique was initiated by the Turbine Branch of Air Force Research Laboratory. Subsequently, a feasibility study was conducted by the PI under the sponsorship of the Turbine Branch and the AFOSR Summer Faculty Research Program (Cao, 1997). Figure 1.1 schematically illustrates a proposed turbine disk with a number of radially rotating heat pipes embedded in the disk (Cao et al., 1998). The heat pipes are circumferentially arranged and extend radially from the disk rim towards the inner radius of the disk. For a gas turbine employing the traditional dovetail attachment, the maximum disk temperature usually occurs near the tip of the dovetail. As a result, the heat pipe is extended as close to the dovetail tip as possible provided that strength considerations are satisfied. A heat pipe arrangement of the type under consideration is elaborated in detail A of Fig. 1.1. The spaces between the individual heat pipes could be reserved, among other considerations, for rotor blade cooling air passages. For the disk shown in Fig. 1.1, a number of individual heat pipes are employed. The independence of each heat pipe increases the reliability of the disk cooling system. However, heat pipe filling and processing may be costly if the number of the heat pipes in a disk is large. Figure 1.2 presents a revised disk heat pipe design. It incorporates a circumferential slot and a number of heat pipe branches. As indicated in the figure, the circumferential slot is located near the inner radius of the disk. Through this slot, the individual heat pipe branches are interconnected. As a result of this interconnection, the whole disk becomes a single heat pipe that can be processed and filled with working fluid only once, and the fabrication cost of the disk could be substantially reduced.

Heat pipes in general are passive heat transfer devices that may have an effective thermal conductance hundreds of times higher than the thermal conductivity of copper.

The heat pipe in the present application is the radially rotating heat pipe, in which the liquid return is facilitated through the rotation-generated centrifugal force. The effective thermal conductance of low-temperature miniature heat pipes with water as the working fluid is on the order of 100 to 200 times that of copper, as evaluated by Cao et al. (1997) from their experimental dada based on the cross-sectional area of the vapor space. The miniature heat pipes to be used in the disk cooling are rotating high-temperature heat pipes with a liquid metal as the working fluid, which in general have a much higher heat transfer capacity compared to that of low-temperature heat pipes. The high-temperature miniature heat pipe has also been proposed for the cooling of turbine rotor blades. The effective thermal conductance of the high-temperature miniature heat pipe excluding the shell effects, as evaluated from the results of Cao (1997), is on the order of 500 to 1,000 times that of copper. This in turn is more than 5,000 to 10,000 times the thermal conductivity of commonly used disk materials. The incorporation of the heat pipe that has such a high thermal conductance is expected to increase the thermal conductance of the disk dramatically while occupying a reasonably small amount of volume in the disk.

On the basis of disk strength considerations, the radius of the heat pipe is considered to be one the order of 2 mm. The heat pipe with this diameter belongs to the miniature range. Like many other devices, heat pipes can be classified as conventional, miniature, and micro heat pipes. The parameter that is used for the classification is the heat pipe interior diameter for circular heat pipes or hydraulic diameter for noncircular heat pipes. For conventional heat pipes, the interior diameter of the heat pipe is on the order of 10-20 mm. For the micro heat pipe that is considered to be used in electronic packaging, the interior diameter of the heat pipe is on the order of 100 μm. However, as

the size of the heat pipe is shrunk, the heat pipe wall would exert tremendously large shear stresses to both vapor and liquid flows in the heat pipe. As a result, the heat transfer capacity of the micro heat pipe is substantially reduced. On the other hand, a heat pipe with a conventional size would not be practical either for the present application. This type of heat pipe would occupy too much space in the disk and subsequently reduce the strength of the turbine disk. The strength consideration is especially important to military gas turbine disks that work at a very high rotating speed and are subject to a high centrifugal force. For the miniature heat pipe, however, the scaling laws would lead to an optimal performance of the heat pipe on the reduced size scale. Unlike the micro heat pipe, the heat transfer capacity of the miniature heat pipe would not be significantly affected by the miniature size and the fabrication of the heat pipe would not face the difficulties that would be encountered when a micro heat pipe is to be manufactured. In addition, the miniature heat pipe would have the advantage of small volume and mass over the conventional heat pipe and would not adversely affect the structure integrity of the turbine disk.

Although the feasibility of the proposed turbine disk has been established and the concept of employing radially rotating heat pipes is well received, experimental demonstrations are needed for the transition of this new concept into real products. Also, the proposed turbine disk structures are preliminary in nature and the analysis undertaken is simplified. To further appreciate the proposed concept, more comprehensive analyses and optimization for the turbine structure are needed. In addition, before the proposed miniature heat pipes are actually applied to military gas turbine engines and advanced

rotating electrical machines, the heat pipes must be fully analyzed and experimentally demonstrated.

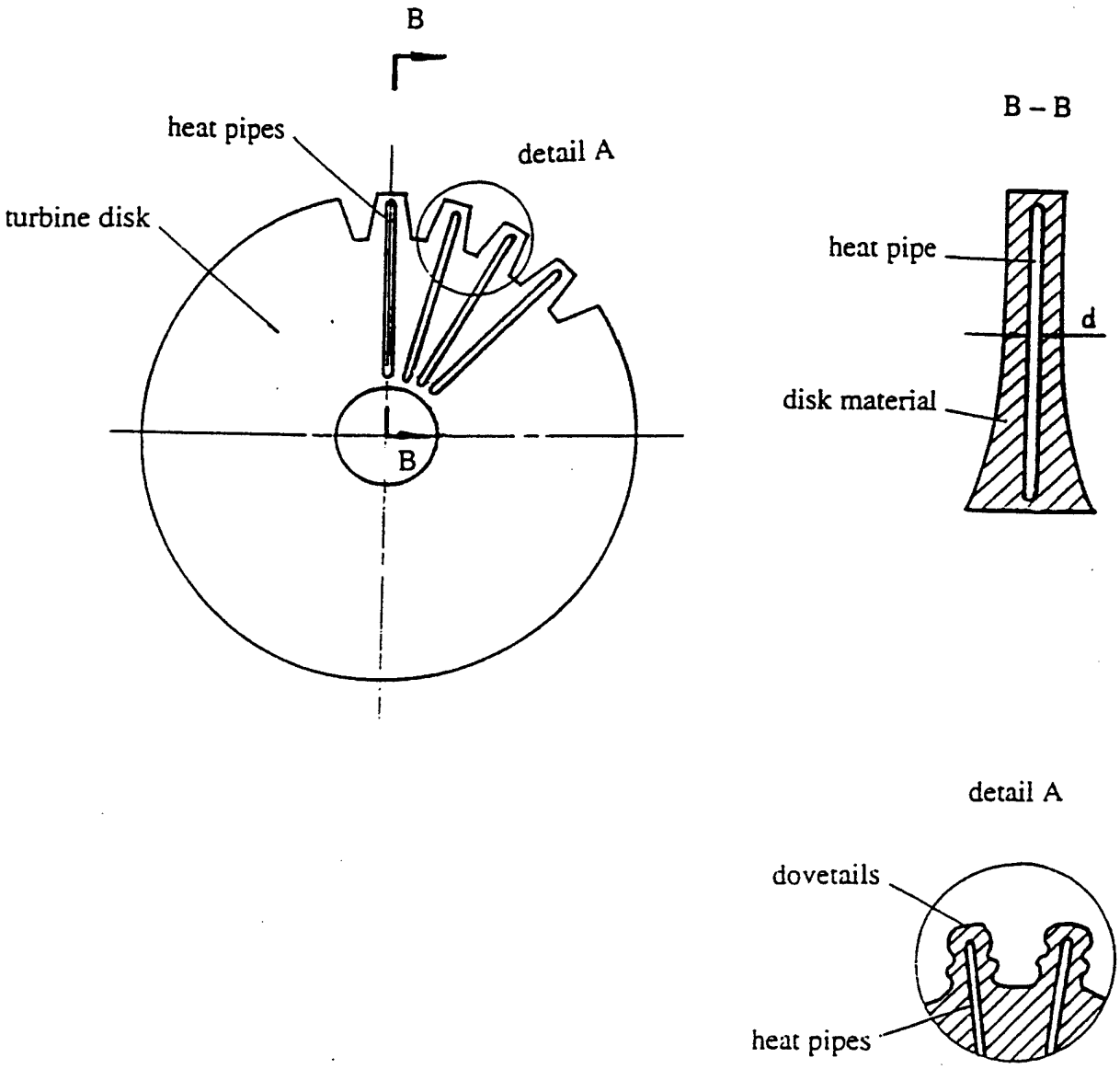

Fig. 1.1 Schematic of a turbine disk incorporating a number of individual radially rotating heat pipes.

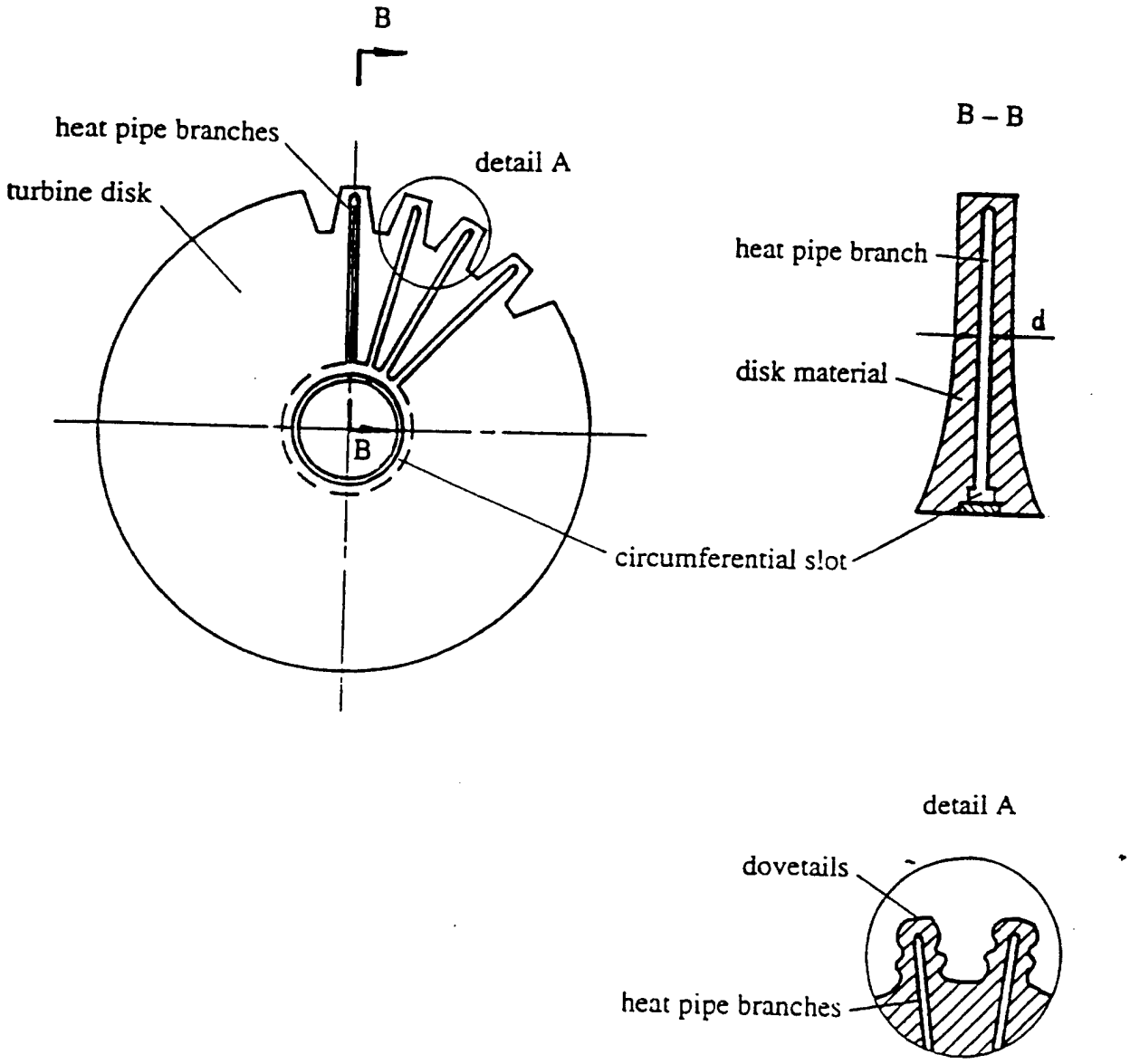

Fig. 1.2 Schematic of a turbine disk incorporating a single heat pipe with a number of interconnected heat pipe branches.

2. EXPERIMENTAL INVESTIGATION OF MINIATURE HEAT PIPES

2.1 High-Speed Rotating Test Apparatus

A high-speed rotating test apparatus specially built for the experimental investigation is shown in Fig. 2.1. For this particular apparatus, the major parameters which could be adjusted in the experiment are the revolution of the test apparatus, heat pipe operating temperatures, heat inputs to the evaporator section, and cooling-air flow rate in the condenser section. The vibration of the apparatus should also be controlled to ensure a safe operation. The shaft is driven by a motor [1] having a revolution range up to 3,600 rpm. In order to dampen the vibration of the rotor, a flexible coupling [18] is used to connect the shaft with the motor. The springs [3] connecting the rotor and frame would have a significant dampening function when the rotor system has a slight unbalance which causes vibration. As a result, the rotating test apparatus constructed is of certain self-balance capability. Two slip-ring assemblies [7] are mounted on the shaft. One is used to supply the electrical current from the power transformer to the heater [15] that provides the heat input to the heat pipe evaporator, and the other is used to feed the temperature data from the thermocouples mounted on the heat pipe shell to the data acquisition system. The rotor disk of the apparatus consists of an inner cylinder [10] and an outer cylinder [11]. The inner cylinder is mounted on the shaft, and the outer cylinder is in turn fixed on the inner cylinder. The radially rotating miniature high-temperature heat pipe [14] is mounted in the outer cylinder. To balance the rotor system, a counter weight [9] is also mounted in the cylinder opposite the heat pipe. The heater cap [12] connected to the outer cylinder has two functions: one is for the protection of the heater, and the other is for adjusting the cooling-air flow rate over the condenser section through

the adjustment of the cooling-air flow window on the heater cap. The flow rate of the cooling air can be calculated by the average relative velocity that the cooling air flows through the window and the area of the window. If the diameter of the outer cylinder is extended, the rotating radius of the heat pipe could be increased.

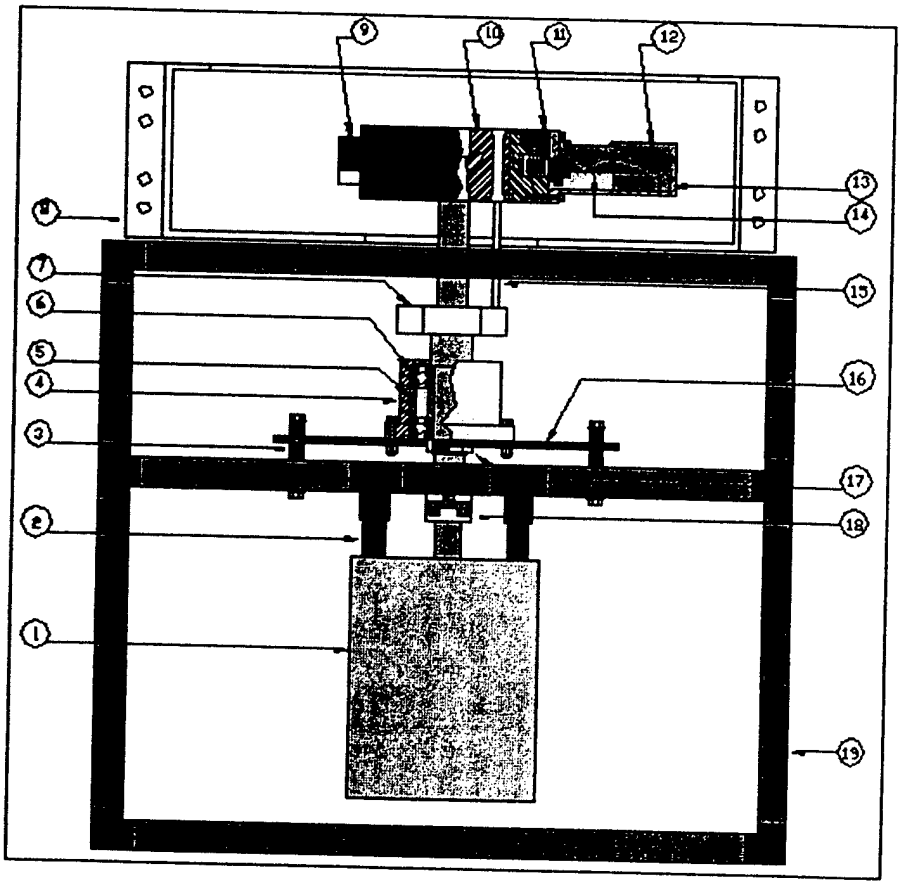

Fig. 2.1 Schematic of the rotating experimental apparatus.

2.2 Experimental Study of Heat Transfer Limitations

It is well known that the condensate in the condenser section is returned to the evaporator section by the centrifugal force in a radially rotating heat pipe. The question is: what would be the smallest centrifugal force under which the condensate can just return to the evaporator section and the heat pipe can still work? This also represents the

critical working limitation of a disk incorporating radially rotating heat pipes. Another limitation of a radially rotating heat pipe is the flooding limitation. During the operation of a heat pipe, the liquid and vapor flow in opposite directions inside the heat pipe. The interaction between the countercurrent liquid and vapor flows occurring at the liquid/vapor interface may inhibit the return of liquid to the evaporator. When this occurs, the heat pipe is said to have reached the flooding limitation. On the other hand, with an increase in the heat input, the velocity of the vapor will increase, which may cause the liquid flow to become unstable. In the most severe case, waves may form at the liquid surface and the interfacial shear forces may become greater than the liquid surface tension, resulting in liquid droplets being picked up or entrained by the vapor flow and carried to the condenser. This entrainment of liquid droplets can limit the axial heat flux and is referred to as the entrainment limit. Since the invention of the heat pipe, many researchers have investigated the flooding/entrainment limit. These investigations are either based on semi-empirical analyses employing the Weber number or empirical correlations. The investigations mentioned above, however, cannot be applied to radially rotating heat pipes due to different condensate return mechanisms in the heat pipe. As a result, it is necessary to conduct investigations for the flooding or entrainment limit of the radially rotating heat pipe. Although these tests could be done based on high-temperature heat pipes, the test of high-temperature heat pipes for the critical working limitation or flooding/entrainment limitation would raise safety concern. Due to the low centrifugal force and high heat input near the critical working limitation, the temperature would increase sharply in the evaporator section and may exceed the metallic melting-point of the heat pipe shell. Because of this reason, copper-water heat pipes are used for the

determination of these working limitations. The experimental data from the water heat pipes could be extrapolated in conjunction with some experimental data from high-temperature heat pipes to determine the working limitations of high-temperature radially rotating heat pipes.

In this study, three copper-water rotating heat pipes having inner diameters of 1.5, 2, and 3 mm, respectively, are fabricated and tested. These heat pipes are tested to prove their reliability, high effective thermal conductance, and the critical working limitation. The experimental data can then be used to generate correlation for the critical working limitation of high-temperature heat pipes. The tests of these water heat pipes could also explore potential applications of radially rotating heat pipes for disks/blades of a high-pressure compressor.

The performance of a copper-water heat pipe is first validated by comparing its performance with that of a copper bar having the same inner and outer diameters. Figure 2.2 shows the temperature distributions along the axial location of a heat pipe and a copper bar. The temperature drop of the heat pipe is much smaller compared to that of the copper bar. It should be noted that the heat input to the heat pipe is twice as much as that to the copper bar for the temperature distributions as illustrated in Fig. 2.2, indicating that the heat pipe works very well. Like a high-temperature heat pipe, a water-copper heat pipe would experience a startup process after the heat is added to the evaporator. Figure 2.3 shows typical temperature distributions of a water heat pipe during the startup procedure. As expected, the heat pipe starts up smoothly and successfully. The time needed for a complete startup is much shorter compared to that of a high-temperature heat pipe.

The working temperature of the present water-copper heat pipe is expected to be well above 100°C. A water heat pipe without air evacuation is still expected to work under this condition albeit with a degraded performance. Figure 2.4 illustrates the temperature distribution of a heat pipe without the air evacuation, along with the temperature distribution of an air-evacuated heat pipe. As can be seen, the performance of the heat pipe without air evacuation degrades somewhat with a larger temperature drop along its length. Still, the temperature drop is much smaller compared to that of a copper bar although the heat input to the copper bar is only one half that of the heat pipe. This means that the performance of a water heat pipe under the turbine engine cooling environment could be reliable even with some non-condensable gas remaining in the heat pipe.

The heat pipe diameter is expected to influence the performance of a heat pipe. Figure 2.5 shows the temperature distributions along the heat pipe length for heat pipes having different diameters. As can be seen, a heat pipe having a larger heat pipe diameter experiences a smaller temperature drop due to smaller resistances to the vapor and liquid flows inside the heat pipe. When the heat pipe diameter is decreased, however, the temperature drop across the heat pipe length is increased substantially, indicating that the heat transfer limitation is being reached under the given heat input and rotating speed. This trend is also shown in Fig. 2.6 under different rotating speeds.

Figure 2.7 illustrates the performance of a heat pipe having a diameter of 2 mm under different heat loads. The temperature level along the heat pipe is higher when the heat input is higher due to the convection boundary condition in the condenser section. However, the temperature drops along the heat pipe differ little indicating that the heat

pipe still performs well at a higher heat input. The heat transfer limitation has not been reached with these heat loads. The results indicated that the heat transfer capacity of the radially rotating heat pie is rather high. It is expected that a radially rotating heat pipe would normally not encounter any catastrophic heat transfer limitation under high-rotating speed turbine conditions. The same conclusion has been reached by the analytical study of Cao and Chang (1997).

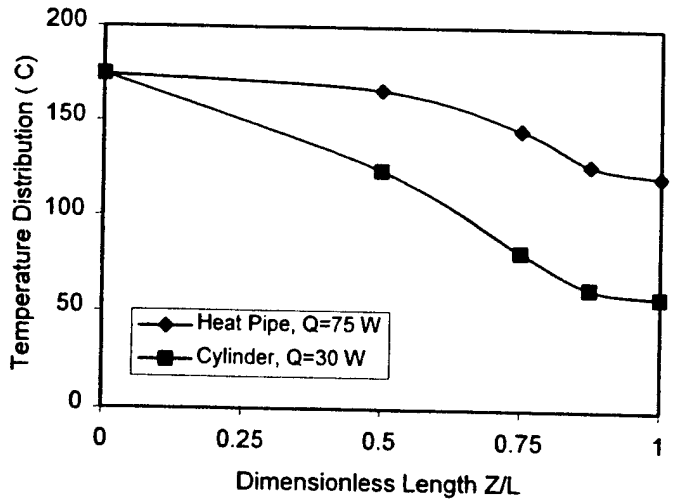

Fig. 2.2 Comparison of the heat pipe and copper bar having the same outer and inner diameters, do =6.4 mm, d_i =1.5 m

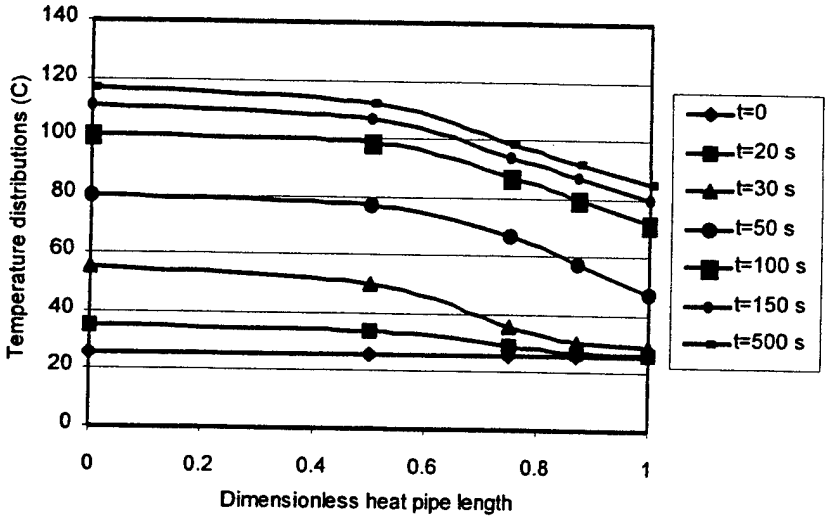

Fig. 2.3 The startup process of a radially rotating heat pipe (Q=50 W, f=30 Hz, d_i=2 mm).

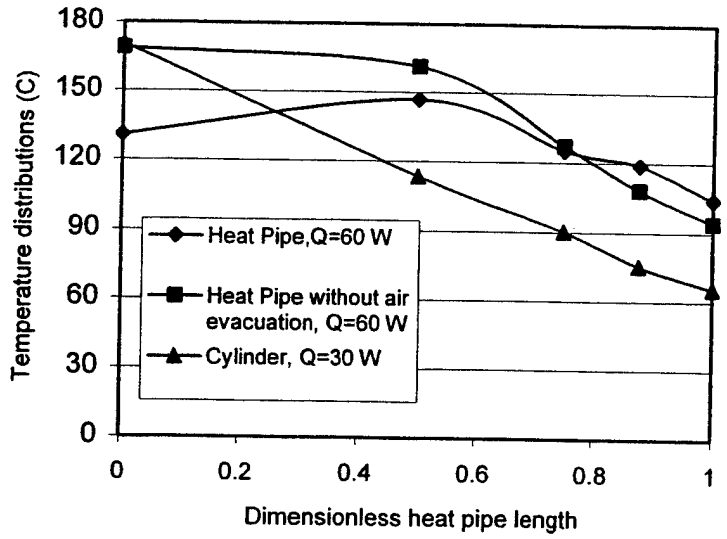

Fig. 2.4 Comparisons of temperature distributions for the heat pipe, heat pipe without air evacuation, and copper cylinder with the same geometrical size and cooling conditions (f=30 Hz, di=2 mm).

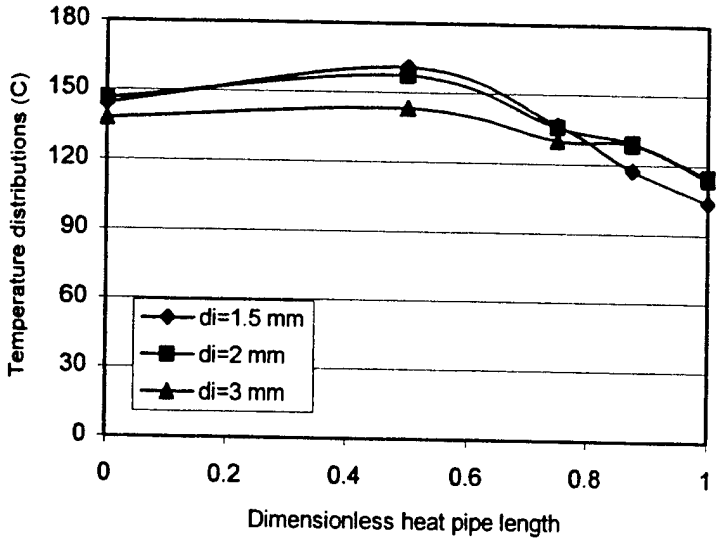

Fig. 2.5 Comparisons of temperature distributions for the heat pipes with different diameters under the same cooling condition (f = 30 Hz, Q = 70 W)

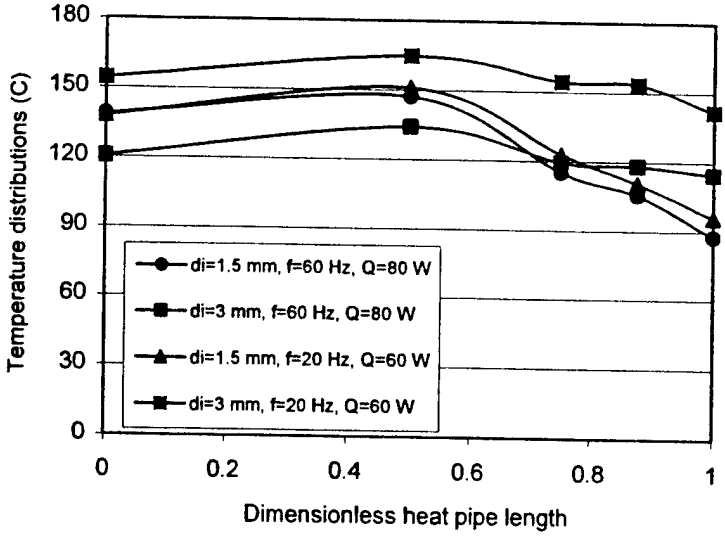

Fig. 2.6 Temperature distributions along dimensionless heat pipe length with different heat inputs and heat pipe diameters.

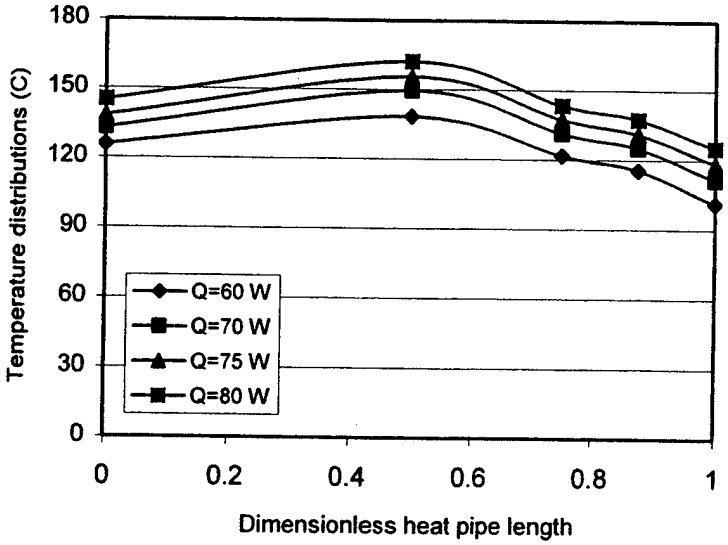

Fig. 2.7 Temperature distributions along dimensionless heat pipe length with different heat inputs and under the same cooling conditions (*di*=2 mm, *f*=35 Hz).

2.3 Experimental Results and Startup Behavior of High-Temperature Heat Pipes

In this section, the experiment results of high-temperature heat pipes are presented. In general, gas turbine blades are made of nickel-based alloys. Considering the high costs and difficulty in fabrication of the heat pipe using a nickel-based alloy, the heat pipes tested are high-temperature sodium/stainless steel (Type 304W) heat pipes. Two radially rotating miniature high-temperature heat pipes of 80 mm in length were designed. One has an inner diameter of 1.5 mm and the other 2 mm. To facilitate sodium charge for the heat pipe, a reservoir with a diameter of 4 mm and length of 5 mm was designed on top of the heat pipe evaporator section. The two heat pipes have the same outer diameter, 6 mm, and the same evaporator and condenser lengths, 40 mm. Four circular fins were manufactured on the outer surface of the condenser section to enhance the convection heat transfer in this region. To install the heat pipe onto the rotating disk, threads were machined at the condenser end so that the heat pipe could be screwed into

the outer cylinder of the high-speed rotating test apparatus. The sodium charge for the heat pipes was undertaken by Thermacore, Inc. For the heat pipe with an inner diameter of 1.5 mm, the sodium charge was approximately 0.06 g, and the sodium charge for the other heat pipe with an inner diameter of 2 mm was approximately 0.08 g.

Five thermocouples of type K were used to measure the heat pipe temperature distribution along the heat pipe length. Two thermocouples were installed at the end cap and the outlet of the evaporator section, respectively, to measure the temperatures in the evaporator section, and the other three thermocouples were mounted in the condenser section to measure the temperature distribution in that section. The heater was mounted on the evaporator sections firmly, and the insulation material of about 16 mm in thickness was clamped between the heater cap and heater to reduce the heat loss from the heater to the surroundings.

To illustrate the effectiveness of the heat pipe, Fig. 2.8 show the comparisons between the experimental data along the heat pipe length and the temperature distributions along a heat pipe container (the heat pipe shell without charging any working fluid) with the same flow rate of cooling air, dimensionless centrifugal forces, and geometrical dimensions. The same experimental data are also shown in Table 2.1. It can be seen from Fig. 2.8 that the heat transfer capacity of the heat pipe container is very low, which is 47 W for the container with an inner diameter of 2 mm, and 60 W for that of 1.5 mm. The temperature distributions along most of the container length are approximately linear, and the temperature in the portion near the end of the container is close to the temperature of the cooling air. For the heat pipes under the same operating conditions, much more heat can be transferred, which is up to 280 W for the heat pipe

with an inner diameter of 2 mm, and 250 W for that of 1.5 mm. If the thermal conductivity of the copper is taken to be 386 W/m-^{o}C, the effective heat conductance of the heat pipes is about 60-100 times higher than the thermal conductivity of copper. This is in turn about 1,000–1,700 times higher than the conductivity of the stainless steel used as the shell in the current study. These comparisons from Fig. 2.2 prove that radially rotating miniature high-temperature heat pipes can work very effectively and reliably. Their heat transfer capacities are much higher than any metals available.

From the experimental data shown in Fig. 2.8, the temperature distribution along the evaporator section and most of the condenser section are nearly uniform. It indicates that the heat pipe works perfectly in these sections. However, there exists a larger temperature gradient near the end cap of the condenser. The large temperature gradient may be attributable to the non-condensable gases remaining in the heat pipe that was swept to the condenser end cap by the vapor flow. It is believed that during the sodium charging process, the air was not completely driven out of the heat pipe before the sealing of the heat pipe. In addition, the condenser end is mounted onto the outer cylinder of the high-speed rotating test apparatus with a screw thread. A large, extra heat sink is thus formed at the condenser end, and some heat from the condenser end is directly transferred into this heat sink. As a result, the heat pipe temperature near the condenser end is forced to stay at a low level close to the temperature of the outer cylinder.

Figure 2.9 illustrates typical temperature distributions of the two heat pipes along the heat pipe length in the process of heat pipe startup. At $t = 0$, a heat input of about 176 W was applied suddenly to the heat pipe evaporator section through the heater described earlier. At the initial moments, the temperatures along the heat pipe length were

unaffected because of the retardation of the heat transfer from the heater to the heat pipe, as shown in Fig. 2.9. With an increase in time, the temperatures in the center of the evaporator section rose faster than those near the end cap of the evaporator, and the condenser sections were still at a temperature close to the ambient temperature. Because the evaporator end has a larger metal mass and holds almost all of the solid sodium, it needs to absorb more heat to raise its temperature. In general, this phenomenon, in which the temperature at the outlet of the evaporator section was higher than that at the end cap of the evaporator, lasted only about 60 seconds. After that time, the temperature at the end cap of the evaporator rose higher than that at the outlet of the evaporator section, and the temperature in the condenser section increased gradually due to the axial heat conduction along the container wall. As the temperature in the evaporator section was further increased, the sodium in the evaporator section was vaporized. The generated vapor flowed from the evaporator section to the condenser section, and the heat pipe started to be operational. As a result, the temperatures along the heat pipe length rose quickly. After about 800-1200 seconds, the temperature distribution along the heat pipe length reached a steady state and the process of the heat pipe startup was completed. Similar to the startup of a high-temperature heat pipe under a non-rotating condition (Faghri et al., 1991), the startup behavior of the current rotating heat pipe is frontal in nature with a sharp drop off in temperature across the vapor front and no pressure recovery in the condenser.

As mentioned earlier, several parameters would significantly influence the performance of the heat pipe. These parameters and their influence on the heat pipe performance are examined next. Fig. 2.10 shows the steady-state temperature

distributions along the heat pipe length with different heat inputs for both heat pipes. At a low heat input in the evaporator section, most of the condenser section remains inactive with its temperature close to the cooling-air temperature. As the heat input is increased, the active zone expands from the evaporator section into the condenser section towards the condenser end cap. The active length of the condenser at the steady state is determined by the surface area necessary to reject the heat applied in the evaporator section. With a low heat input and a relatively high rotating speed, which would provide a high heat transfer coefficient, only a small portion of the total condenser surface area is needed to reject the applied heat. As a result, most of the condenser would remain inactive at the steady state when the heat input is low. In the current experiment, the inactive part of the condenser may also be attributable to the existence of non–condensable gas remaining in the heat pipe.

When the flow rate of cooling air, dimensionless centrifugal force, and inner diameter of the heat pipe are fixed, the operating temperatures in the evaporator section will be increased with an increase in the heat input, and consequently the temperature along the condenser section will go up, as shown in Fig. 2.10. Accordingly, the heat transfer characteristics and effective thermal conductance will be improved significantly. When the heat input is further increased and reaches about 300 W for the heat pipe with an inner diameter of 2 mm, as shown in Fig. 2.11, the temperature distribution stays relatively uniform until reaching the region close to the condenser end. Also, a temperature peak emerges near the condenser end, as shown in Fig. 2.11. With an increase in the heat input, a large amount of vapor is generated in the evaporator section and the vapor flows with a high speed towards the end of the condenser section. Because

of this high speed, the vapor flow has reached the sonic limitation, and vapor compressibility then takes effect. The vapor continues to expand in the condenser section, which is followed by a pressure recovery. Owing to the effect of non-condensable gases and the heat sink at the condenser end, the temperature at the condenser end is forced to stay at a relative low temperature. As a result, a temperature peak would appear near the end of the condenser section. It should be pointed out that this sonic limit could become higher if the heat pipe is to work at a higher temperature level.

Flow rate of the cooling air in the condenser section has a dominant influence on the operating temperature level of the heat pipe. As the flow rate of the cooling air is increased, the convective heat transfer coefficient at the outer surface of the condenser section is increased. Therefore, the heat transfer capacity at the outer surface of the heat pipe is increased. If the heat input is kept at a constant, as the cooling air flow rate is increased, the operating temperature of the heat pipe will be decreased, the working section of the condenser will be shortened, and the temperature distributions along the condenser section will become less uniform near the condenser end. In this case, when the operating temperature is too low and the heat input is too high, the sonic limit of the heat pipe will be reached.

Fig. 2.12 compares the temperature distributions along the heat pipe length with different cooling-air flow rates when the temperature of the cooling air is kept at 30°C. It can be seen from the figure that, for the same heat input and dimensionless centrifugal force, the temperature along the heat pipe length is increased with a decrease in the flow rate of the cooling air. Due to this increased heat pipe temperature, the vapor pressure is accordingly increased. At the same time, the non-condensable gases in the heat pipe are

more likely to be compressed towards the condenser end owing to the increased vapor pressure. As a result, the non-condensable gases would occupy a smaller portion of the condenser section, and the temperature distribution near the condenser end would become more uniform.

At a higher revolution or rotating frequency, the dimensionless centrifugal force plays a dominant role in the temperature drop along the heat pipe length. With an increase in the dimensionless centrifugal force, the vapor pressure and temperature drops along the heat pipe length will be increased. Therefore, to some degree, the dimensionless centrifugal force dominates the slope of the temperature distribution and the temperature drop along the heat pipe length.

Although the dimensionless centrifugal force has a similar effect on the total temperature drop along the heat pipe length compared to that of the cooling-air flow rate, the mechanisms that cause the change of the temperature drop are different. As the cooling-air flow rate is increased, the convection on the outer surface of the condenser section will be intensified, the working section of the condenser will be shortened, and the temperature gradient along the condenser length will become steeper. But the slope of the temperature distribution along the evaporator section would remain a constant. On the other hand, when the dimensionless centrifugal force is increased, the temperature drop caused by the vapor centrifugal force will be increased, and the total temperature drop including that in the evaporator section will be increased.

Fig. 2.13 shows temperature distributions along the heat pipe length at different rotating frequencies. As shown in the figure, at a low rotating frequency, $f = 30$ Hz, which corresponds to a dimensionless centrifugal force, $\omega^2 \overline{Z}_a / g$, of 470, the slopes of

the temperature distributions along the evaporator section are relatively small and temperature distributions in the evaporator section are relatively uniform. When the rotating frequency is increased from f = 30 Hz to 60 Hz, the slope of the temperature distribution in the evaporator section becomes steeper with an increased temperature drop in the evaporator section.

Fig. 2.14 shows the comparisons of temperature distributions along the heat pipe length for the two heat pipes with inner diameters of 2 mm and 1.5 mm, respectively. It is evident that the temperature drop along the heat pipe with an inner diameter of 1.5 mm is larger than that with an inner diameter of 2 mm when the heat input, dimensionless centrifugal force, and flow rate of cooling air are kept at constants. On the other hand, the operating temperature in the evaporator section of the heat pipe is higher when the inner diameter is smaller. This is because a higher pressure drop is needed to overcome the friction of vapor flow in the heat pipe having a smaller inner diameter. Accordingly, the saturated temperature in the evaporator section of the heat pipe having a smaller inner diameter is higher. This trend would be more evident with a further decrease in the inner diameter of the heat pipe.

Table 2.1 Comparisons of the temperature distributions and heat inputs between the heat pipe and heat pipe container with the same geometry.

Dimensionless heat pipe length z/L	Temp. distribution of the heat pipe (di=2 mm) (°C)	Temp. distribution of the heat pipe container (di=2 mm) (°C)	Temp. distribution of the heat pipe (di=1.5 mm) (°C)	Temp. distribution of the heat pipe container (di=1.5 mm) (°C)
0.000	830.0	814.2	786.0	801.5
0.500	821.8	382.1	776.4	413.5
0.750	804.4	79.5	766.2	91.8
0.875	742.4	42.0	698.4	48.2
1.000	390.0	37.9	354.3	35.3

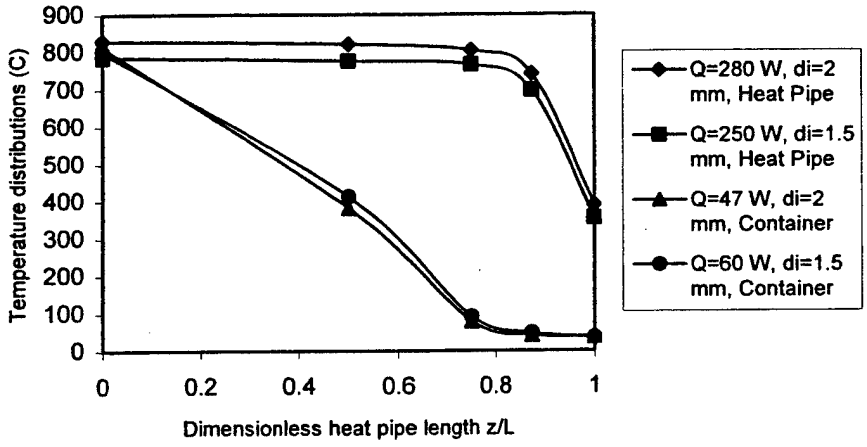

Fig. 2.8 Comparisons of temperature distributions and heat inputs between the heat pipe and the heat pipe container ($\omega^2 \overline{Z}_a / g$ =470, and W=6.7×10^{-3} m^3/s).

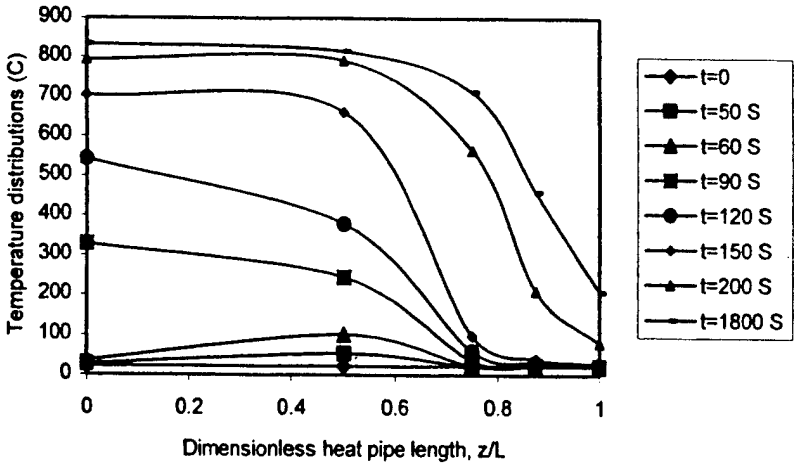

(a) $\omega^2 \overline{Z}_a / g = 470$, d_i=1.5 mm, Q=176 W

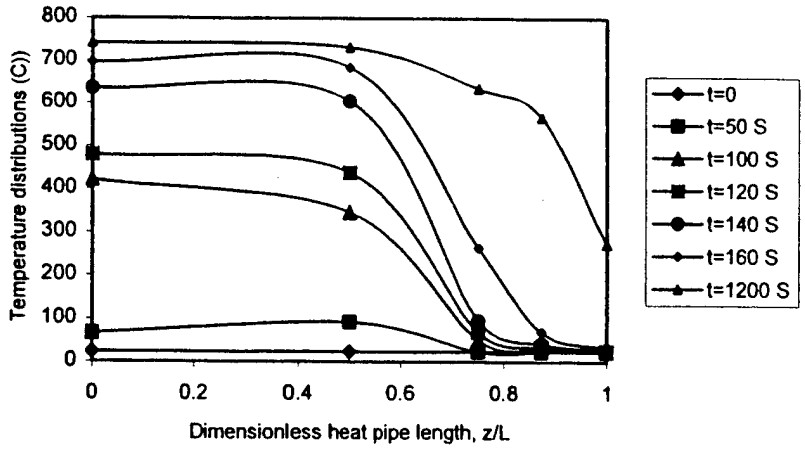

(b) $\omega^2 \overline{Z}_a / g = 470$, d_i=2 mm, Q=175 W

Fig. 2.9 Temperature distributions along the heat pipe length with the diffuse effects of non-condensable gases during the heat pipe startup process.

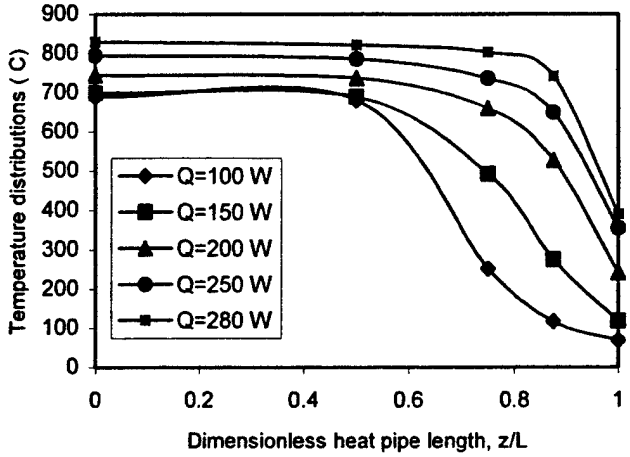

(a) $\omega^2 \overline{Z}_a / g = 470$, d_i=2 mm, W=$6.7\times10^{-3} m^3/s$

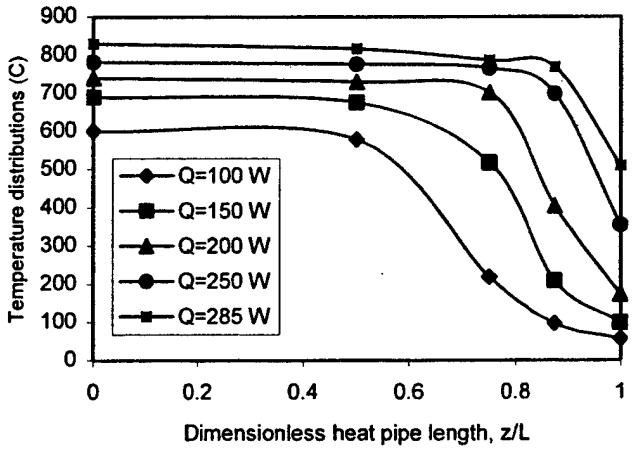

(b) $\omega^2 \overline{Z}_a / g = 470$, d_i=1.5 mm, W=$6.7\times10^{-3} m^3/s$

Fig. 2.10 Temperature distributions along the dimensionless heat pipe length with different heat inputs.

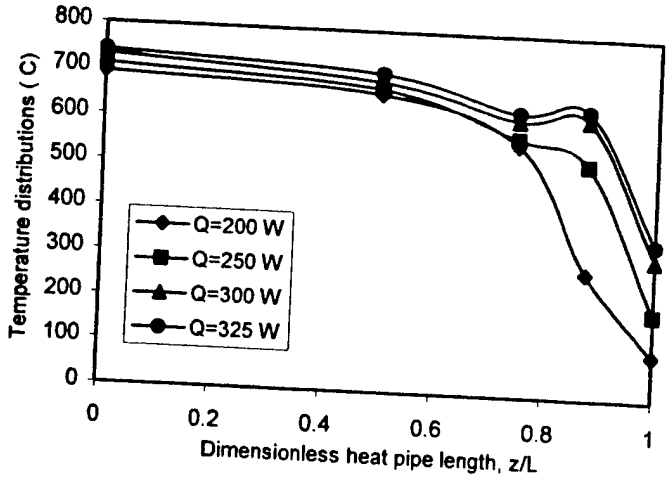

(a) $\omega^2 \overline{Z}_a / g$ =1306, d_i =2 mm, W=11.2×10^{-3} m^3/s

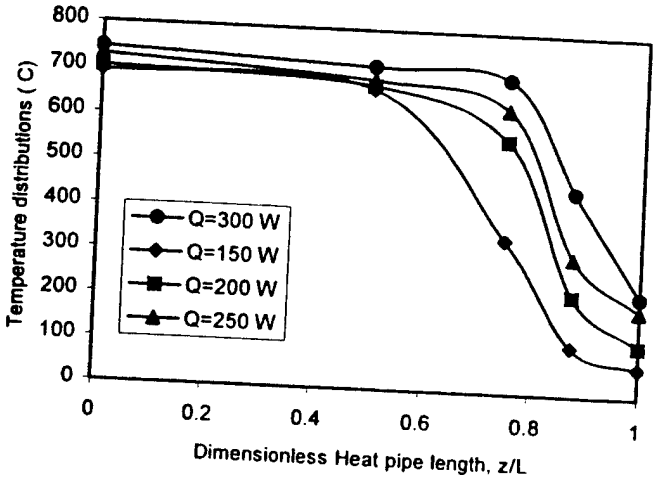

(b) $\omega^2 \overline{Z}_a / g$ =1881, d_i =2 mm, W=13.4×10^{-3} m^3/s

Fig. 2.11 Temperature distributions along the dimensionless heat pipe length with different rotating frequencies and flow rates of the cooling air.

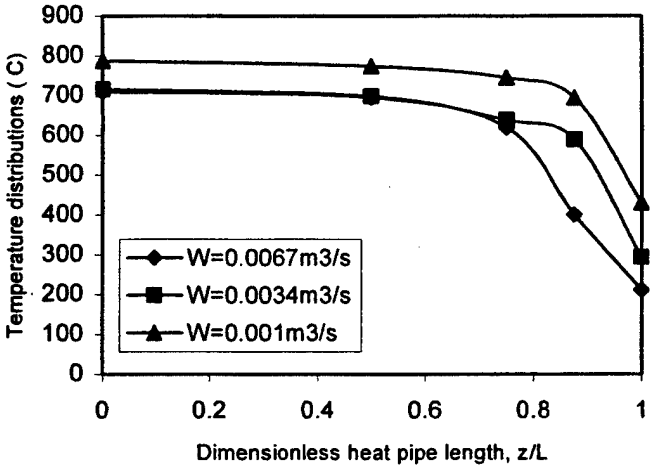

(a) $\omega^2 \overline{Z}_a / g$=470, d_i=2 mm, Q=200 W

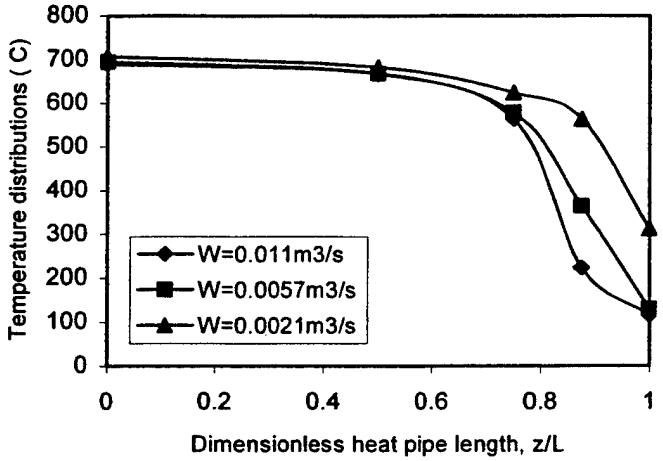

(b) $\omega^2 \overline{Z}_a / g$ =1306, d_i=2 mm, Q=200 W

Fig. 2.12 Comparisons of temperature distributions along the dimensionless heat pipe length with different flow rates of the cooling air.

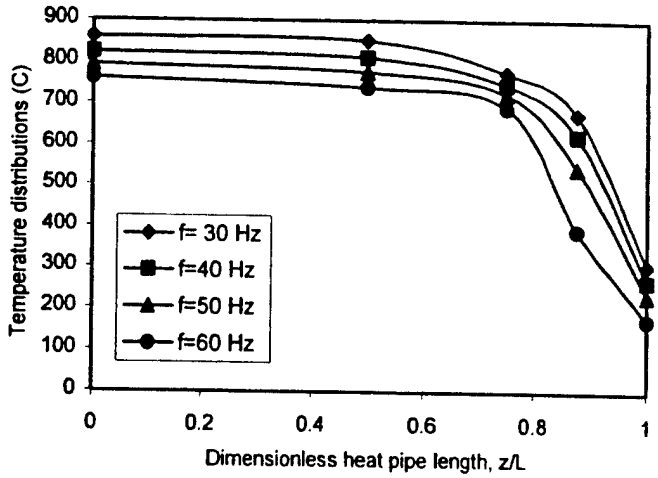

(a) Q=225 W, d_i =1.5 mm

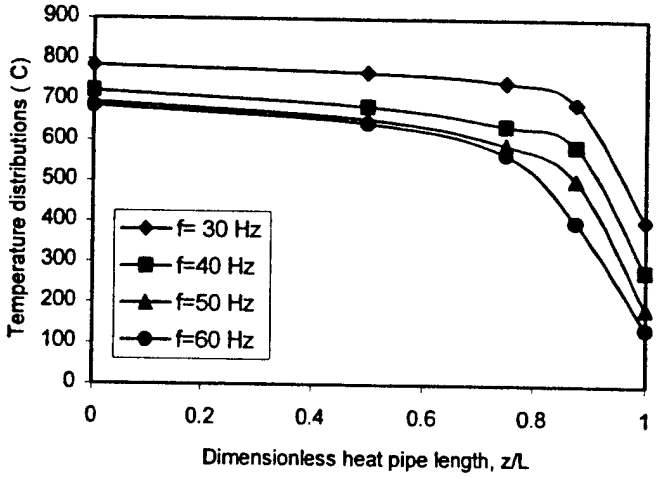

(b) Q=225 W, d_i =2 mm

Fig. 2.13 Temperature distributions along the dimensionless heat pipe length with different rotating frequencies and flow rates of the cooling air.

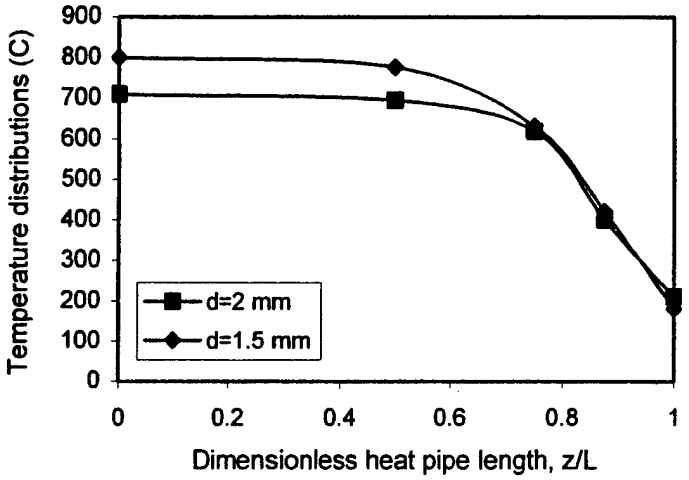

(a) Q=200 W, $\omega^2 \overline{Z}_a / g = 47\,0$, W=$6.7\times10^{-3} m^3/s$

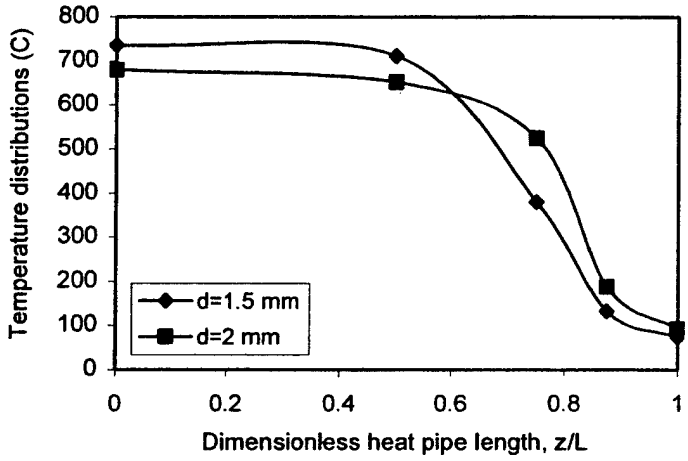

(b) Q=200 W, $\omega^2 \overline{Z}_a / g = 1881$, W=$13.4\times10^{-3} m^3/s$

Fig. 2.14 Comparisons of temperature distributions along the dimensionless heat pipe length with different inner diameters.

2.4 Conclusions

Based on the experimental investigations presented in this section, the following conclusions may be made:

1. The radially rotating miniature heat pipe can work effectively and reliably in the reported laboratory environment, and has a high effective thermal conductance (60-100 times higher than the thermal conductivity of copper).
2. Heat input has a very important influence on the temperature distributions and heat transfer characteristics of the heat pipe. With an increase in the heat input, the temperature level in the condenser sections will go up. Accordingly, the heat transfer characteristics and effective heat conductance of the heat pipe will be improved significantly. However, when the heat input exceeds a certain level, the sonic limit of the heat pipe may be reached.
3. The flow rate of the cooling air in the condenser section has a dominant influence on the temperature distribution of the heat pipe. When the flow rate of the cooling air is increased, the heat transfer capacity at the outer surface of the condenser will be increased. As a result, the operating temperature of the heat pipe will be reduced, the working section of the condenser will be shortened, and the temperature distributions near the condenser end will become steeper.
4. The dimensionless centrifugal force plays an important role in the temperature drop along the heat pipe length especially in the evaporator section. A higher heat pipe rotating speed will increase vapor pressure and temperature drops along the heat pipe length.

5. The inner diameter of a heat pipe determines the cross-sectional area of the vapor flow in the heat pipe. The miniature heat pipe with a smaller inner diameter will have a larger temperature drop along the heat pipe than that with a larger inner diameter when the heat input, flow rate of cooling air and dimensionless centrifugal force are kept the same.

3. NUMERICAL ANALYSES OF GAS TURBINE DISKS INCORPORATING ROTATING HEAT PIPES

3.1 Introduction

Based on the proposed turbine disk incorporating radially rotating heat pipes, Cao et al. (1998) also presented an analytical analysis to evaluate the effectiveness of the heat pipe on the temperature reduction at the disk rim. The analysis is based on the comparison between the disks with and without incorporating the heat pipe. The analytical results indicate that the heat pipe cooling is very effective, which could reduce the disk rim temperature by several hundred degrees under the same working conditions. However, the analysis is based on a one-dimensional assumption and a simplified disk geometry to seek a closed-form solution. Since the heat transfer in a turbine disk is three dimensional in nature with a complex geometry, the assumptions made for the analytical solution could introduce significant errors for the evaluation of the temperature distribution in the disk. To improve the accuracy of the analysis, a comprehensive three-dimensional numerical analysis is needed, which is the subject of the present section.

3.2 Numerical Modeling

Because of the structural symmetry, only a disk sector containing one dovetail is numerically modeled. Fig. 3.1(a) shows such a sector from a conventional reference disk without heat pipes and Fig. 3.1(b) illustrates the same disk sector with the incorporation of radially rotating heat pipes. The disk under consideration has an outer diameter of 500 mm and an inner diameter of 200 mm. The dovetail has a depth of 40 mm and an angle of 20 deg. It should be pointed out that the disk dimensions mentioned above are representative in nature and are used in the numerical calculation only for demonstration purposes. The thermal conductivity of the disk material is taken as 24 W/m-K. To simulate the heat input conditions to the disk, heat is applied at the disk rim and the side surfaces of the dovetail groove, which is denoted by W_1. The cooling conditions on the disk side surface would vary with radial position. To more accurately approach the real cooling condition, the side surface is divided into three segments, W_2, W_3 and W_4. The convection heat transfer coefficients corresponding to these three segments are denoted by h_2, h_3 and h_4, respectively. To simplify the analysis, the heat pipes incorporated in the disk are treated as solid bars having a high effective thermal conductance, k_{eff}. This simplification is the same as that adopted by Cao et al. (1998) and could avoid solving the complicated two-phase flow in the heat pipes. In addition, the heat pipe cannot be placed too close to the disk rim because of structural concerns. As a result, a distance Δs is maintained between the heat pipe top end and the disk rim, as shown in Fig. 2(b).

The governing equation for three-dimensional heat conduction in a solid is:

$$\frac{\partial}{\partial t}(\rho h) = \frac{\partial}{\partial x_i}(k\frac{\partial T}{\partial x_i}) \qquad i = 1, 2, 3 \qquad (3.1)$$

where h is the specific enthalpy and $T = f(\vec{r}, t)$. The thermal conductivity in the above equation should be replaced by k_{eff} in the heat pipe regions. The general boundary condition for heat transfer can be represented by Eq. (3.2):

$$\frac{\partial T}{\partial x_i} = f_i(\vec{r}, t) \tag{3.2}$$

where $f(\vec{r}, t)$ is a function of the position vector and time. The total heat transfer rate at a surface is attributable to both convection and radiation, and can be represented by the following relation:

$$q_i^{"} = h_i \Delta T + q_{rad}^{"} \tag{3.3}$$

Numerical simulations are made by employing the commercially available computer software FLUENT, and SIMPLE algorithm is selected for the numerical calculation. During the simulations, parameters in connection with heat input, air cooling condition, material properties, and heat pipe dimensions are varied within the following ranges:

$10W/cm^2 \le q^{"} \le 50W/cm^2$; $10^3 W/m-K \le k_{eff} \le 5\times10^4 W/m-K$; $k = 24W/m-K$;

$2mm \le \Delta s \le 5mm$; $T_c = 525^oC = 798K$; $60mm \le L \le 140mm$; $3mm \le d_i \le 10mm$;

Cooling conditions at the side surface segments:

Cooling condition 1: $h_2 = 500W/m^2-K$; $h_3 = 350W/m^2-K$; $h_4 = 150W/m^2-K$;

Cooling condition 2: $h_2 = 1000W/m^2-K$; $h_3 = 700W/m^2-K$; $h_4 = 300W/m^2-K$;

Cooling condition 3: $h_2 = 1500W/m^2-K$; $h_3 = 1050W/m^2-K$; $h_4 = 450W/m^2-K$;

Cooling condition 4: $h_2 = 2000W/m^2-K$; $h_3 = 1400W/m^2-K$; $h_4 = 600W/m^2-K$.

Where q'' is the heat flux at the heating surface, Δs is the distance between the disk rim surface and heat pipe top end, T_c is the cooling air temperature, L is the heat pipe length, and d_i is the heat pipe diameter.

3.3 Numerical Results and Discussion

To compare the cooling effectiveness of the heat pipe on the turbine disk, a reference disk without incorporating heat pipes is first simulated, which is schematically shown in Fig. 3.1a. The properties of the disk material, cooling air temperature, heat input at the disk rim and dovetail groove, and the distribution of the heat transfer coefficients between the disk side surface segments and the cooling air are, respectively, $k = 24 W/m-K$, $T_c = 525°C = 798K$, $q'' = 30 W/cm^2$ and cooling condition 3 as presented in section 3.2. The numerical results obtained in connection with the thermal performance of the disk are as follows: the maximum temperature, T_{max}, at the disk rim and dovetail surface, W_1, is 1597 K; the average temperature, T_{avg}, at the same surface is 1352.8 K; the minimum temperature, T_{min}, in the entire disk is 809.9 K; and the average temperature, T_{avg}, at the disk inner surface, W_5, is 810.8 K. These numerical temperature data as well as the heating and cooling conditions from the reference disk without heat pipes are used as the baseline for comparison with those from the disks incorporating heat pipes. However, when the comparison is to be made under a different heating or cooling condition, the temperature distribution will need to be recalculated for the aforementioned reference disk.

3.3.1 Effect of Heat Pipe Diameters

Heat pipe diameters would significantly affect the cooling effectiveness of the heat pipe on the turbine disk. A heat pipe having a larger diameter would have a larger

heat transfer surface and a higher heat transfer capacity. As a result, it can transfer more heat away from the disk rim and dovetail surface, which could result in a lower temperature in these areas for given heat input and cooling conditions on the disk surface.

Figure 3.2 shows the maximum and average temperature reductions at the disk rim with different heat pipe diameters. The results are in terms of $T_n - T$, where T_n is the temperature of the reference disk without the heat pipe and T is the temperature of the disk with heat pipes. The heat pipes employed have a length of 120 mm and an effective thermal conductance, k_{eff}, of 20,000 W/m-K. The distance between the heat pipe top and the disk rim is taken to be $\Delta s = 3$ mm. In later comparisons, the above values for the heating condition, effective thermal conductance of the heat pipe, k_{eff}, and Δs are taken to be the same unless otherwise specified.

It is clear from Fig. 3.2 that with an increase in heat pipe diameter, the reduction of the maximum and average temperatures at the disk rim and dovetail surface increase significantly. For the disk cooled by heat pipes having a diameter of 3 mm, the maximum and average temperatures at the disk rim and dovetail surface are reduced by about 220 K and 120 K, respectively. For the disk having a heat pipe diameter of 10 mm, the maximum and average temperatures are reduced by about 385 K and 225 K, respectively, under the same heating and cooling conditions. These results indicate that the heat pipe with a bigger diameter is especially effective for the reduction of maximum disk rim temperature. The heat pipe would be beneficial for preventing overheating and high-temperature creep at the disk rim and dovetail surface. This conclusion is in good agreement with the analytical study of Cao et al. (1998).

3.3.2 Effect of Heat Pipe Effective Thermal Conductance

The effective thermal conductance of a heat pipe is directly related to the heat transfer capacity of the heat pipe. The analytical study of Cao et al. (1998) indicated that the heat pipe having a higher effective thermal conductance could transfer more heat with a smaller temperature gradient along the heat pipe length and achieve a bigger temperature reduction at the disk rim.

Figure 3. 3 shows the reductions of the maximum and average temperatures at the disk rim and dovetail surface with different heat pipe thermal conductance. The numerical results in the figure indicate that the cooling effectiveness of the heat pipe is relatively low when the effective thermal conductance is below 1,000 $W/m-K$. With an increase in the effective thermal conductance, the cooling effectiveness improves dramatically. When the effective thermal conductance exceeds 20,000 W/m-K, the maximum and average temperature reductions at the disk rim and dovetail surface exceed 300 K and 175 K, respectively, when the heat flux at W_1 is 30 W/cm^2 and cooling condition 3 is chosen. As indicated in the previous section, experimental study has proven that an effective thermal conductance of 20,000 or higher can be achieved for a high-temperature radially rotating miniature heat pipe. However, as indicated in Fig. 4, the improvement of the cooling effectiveness begins to level off after the effective thermal conductance exceeds 10,000 W/m-K. The improvement becomes insignificant when the effective thermal conductance exceeds 20,000 W/m-K. In this case, the heat transfer is dominated by the thermal resistance of the disk material surrounding the heat pipe. Therefore, the effort to seek an even higher thermal conductance of the heat pipe may not be necessary.

3.3.3 Effect of Air Cooling Conditions

The cooling condition on the disk side surface has a significant influence on the temperature distribution in the disk. A favorable cooling condition would result in a lower temperature distribution in the disk. However, the cooling air comes from the compressor and its temperature is predetermined by the compressor design. At the same time, an increase in the flow rate of the cooling air would result in an increase in the power consumption of the compressor and reduce the overall thermal efficiency of the gas turbine engine. As a result, there should be a trade-off between the cooling air flow rate and the temperature distribution in the disk.

Figure 3.4 illustrates the comparison of the maximum and average temperature reductions at the disk rim and dovetail surface under four different cooling conditions, which are defined in the previous section of this section. The comparisons are based on the same heat flux ($q^{"}$=30 W/cm^2), and the heat pipe length and diameter are taken as 120 mm and 5 mm, respectively. It is evident from the figure that the temperature reductions at the disk rim and dovetail surface incorporating the heat pipe are the most significant with an adverse air cooling condition. In the case of cooling condition 4, the temperature reductions for the maximum and average temperatures reach about 430 K and 275 K, respectively. Cooling condition 4 is characterized by the low heat transfer coefficients at different segments of the disk surface, which corresponds to a low cooling air flow rate or low disk rotating speed. It should be pointed out that the above comparisons are based on the temperature difference between the disks with and without incorporating the heat pipe. It does not mean that the worse the cooling condition, the lower the temperature in the disk. In fact, for the disks with and without heat pipes, the

temperatures at the disk rim and dovetail surface are the lowest when the cooling condition is the strongest. As the cooling condition becomes worse, the temperature at the disk rim and dovetail surface will rise sharply. The temperature may still exceed the temperature limitation of the disk material even if the heat pipe in the disk can reduce the maximum and average temperatures effectively compared to those without the heat pipe. As a result, in the practical application, an optimum design based on the cooling condition, power consumption of the compressor, temperature limitation of the disk material, and cooling effectiveness of the heat pipe should be considered.

3.3.4 Effect of Heat Pipe Locations in the Disk

The location of heat pipes in the disk, especially the distance between the heat pipe top and the disk rim, is an influential factor that significantly affects the heat pipe cooling effectiveness. From the view point of heat transfer, if the cooling condition and heat input are fixed, the maximum and average temperatures at the disk rim and dovetail surface will be reduced and the cooling effects will be improved when the location of the heat pipe is closer to the disk rim and dovetail surface. However, the location of the heat pipe must be constrained by the structural and stress consideration of the disk material at the disk rim.

Fig. 3.5 illustrates the cooling effectiveness of the heat pipe with different distances between the heat pipe top and disk rim, Δs. As can be seen from the figure the maximum and average temperature reductions are about 300 K and 170 K, respectively, when the distance between the heat pipe top and disk rim, Δs, is 2 mm. With an increase in the distance, the maximum temperature and average temperature reductions will be decreased, and the cooling effectiveness will be lower. The maximum temperature and

average temperature reductions are about 280 K and 160 K, respectively, when the distance between the heat pipe top and disk rim is 5 mm. The present numerical results indicate that the cooling effectiveness on the disk rim and dovetail surface will not be reduced significantly when the distance varies from 2 mm to 5 mm. Under this condition, the heat pipe is expected to provide sufficient cooling for the disk rim while satisfying the structural and stress consideration.

3.3.5 Effect of Heat Fluxes at the Disk Rim

The heat flux on the disk rim and dovetail surface has a very strong effect on the temperature distribution in the disk. With an increase in the inlet gas temperature of a gas turbine, the heat flux at the disk rim and dovetail surface will be increased accordingly. As a result, the high heat flux would prohibit the increase of the gas temperature for the purpose of improving turbine efficiency, and result in an overheating of the disk material at the rim and dovetail surface, especially for compact aero-engines having a small size.

The comparisons of the maximum and average temperature reductions at the disk rim and dovetail surface are shown in Fig. 3.6 for different values of the heat flux at W_1. It is clear that the cooling effectiveness is relatively small and the maximum and average temperature reductions at the disk rim and dovetail surface are relatively low when the heat flux is low. The temperature reductions, for instance, are about 100 K and 60 K, respectively, when the heat flux is only 10 W/cm^2. Because at a low heat flux, the temperatures at the disk rim and dovetail surface are already relatively low, the importance of employing the heat pipe is reduced and a relatively low reduction of these temperatures employing the heat pipe is expected. But with an increase in the heat flux, the temperature at the disk rim and dovetail surface will rise sharply if the cooling

condition at the disk surface remains the same. At the same time, the cooling effectiveness of the heat pipe will be increased greatly. The maximum and average temperature reductions at the disk rim and dovetail surface approaches about 500 K and 300 K, respectively, when the heat flux reaches 50 W/cm^2. The numerical results in Fig. 3.6 indicate that the heat pipe cooling is the most effective when the gas turbine works at an elevated temperature which results in a high heat flux into the turbine disk. The general tendency of temperature reductions is in good agreement with the analytical solution of Cao et al. (1998). As a result, the cooling technique studied in this section would be especially useful for advanced gas turbine engines that would work at an extremely high temperature.

3.3.6 Effect of Heat Pipe Lengths

The heat pipe is a heat transfer device with a high thermal conductance that can transfer heat effectively from its evaporator to condenser. As a result, the heat pipe length determines the distance over which the heat is transferred. For a disk incorporating heat pipes, the heat pipe length has an important influence on the temperature at the disk inner surface, which would be in contact with the shaft or drum of the gas turbine. Under given cooling and heating conditions, as the heat pipe length is increased, the average temperature on the disk inner surface will be increased. At the same time, the maximum and average temperatures at the disk rim and dovetail surface will be decreased. This is because the heat transfer passage in the disk will be extended and the effective heat transfer area will be increased when the heat pipe length is increased. However, the increase in the temperature at the disk inner surface, which is denoted by W_5 in Fig. 3.1(b), may not be desirable and may need to be contained in some situation.

For a fixed heat flux, $q^{"} = 30$ W/cm^2, and cooling condition 3, the comparison between disks with and without heat pipes for the temperature reductions at the disk rim, $T_r - T$, and the temperature increases at the disk inner surfaces, $T - T_r$, with different heat pipe lengths and two heat pipe diameters is shown in Fig. 3.7. In Fig. 3.7(a), the maximum and average temperature reductions at the disk rim and dovetail surface increase with an increase in heat pipe length. However, after the heat pipe length exceeds 100 mm, a further increase in heat pipe length would not reduce the disk rim temperature further. This means that a heat pipe with a relatively short length will be sufficient for the reduction of the temperature at the disk rim. The use of a relatively short heat pipe will also have the benefit of limiting the temperature increase at the disk inner surface. It can be seen from Fig. 3.7b that when the heat pipe length is around 80 mm, the temperature increase at the disk inner surface for the heat pipe having a diameter of 5 mm is less than 40 K. However, when the heat pipe length is increased, the inner surface temperature is increased substantially. Therefore, the use of a long heat pipe is not desirable or necessary in the present application.

3.4 Conclusions

The use of radially rotating heat pipes is a novel approach for the thermal management of aero-engine disks working under a very high temperature. The disk incorporating the heat pipe would have an enhanced thermal dissipation capacity and much lower disk rim and dovetail surface temperature. Extensive numerical simulations have been made for both disks with and without heat pipes. Various parameters that would affect the cooling effectiveness of the heat pipe are also studied. Numerical results indicate that the maximum disk rim and dovetail surface temperature could be reduced by

about 200 to 400 K depending on the disk working conditions for the disk incorporating the heat pipe. As a result, the disk incorporating radially rotating heat pipes could meet the stringent requirements of small-size and high-heat flux conditions encountered in an advanced aero-engine.

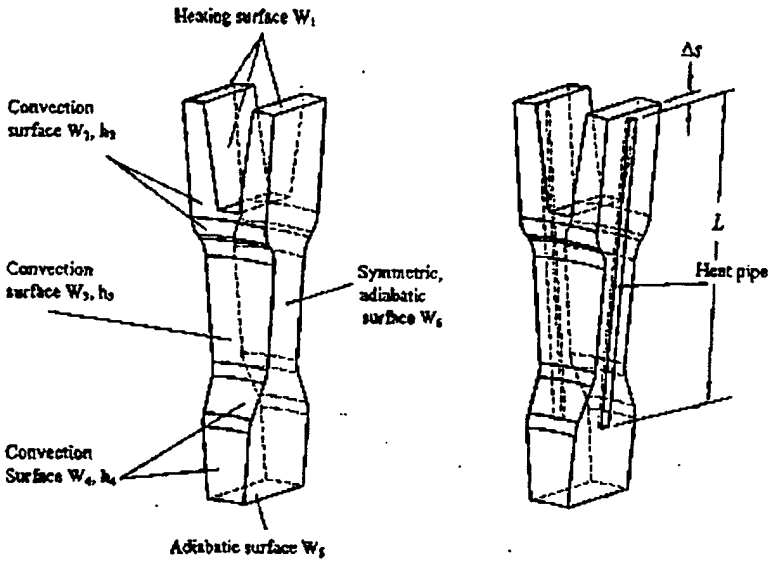

Fig. 3.1 Schematics of turbine disks with and without radially rotating heat pipes.

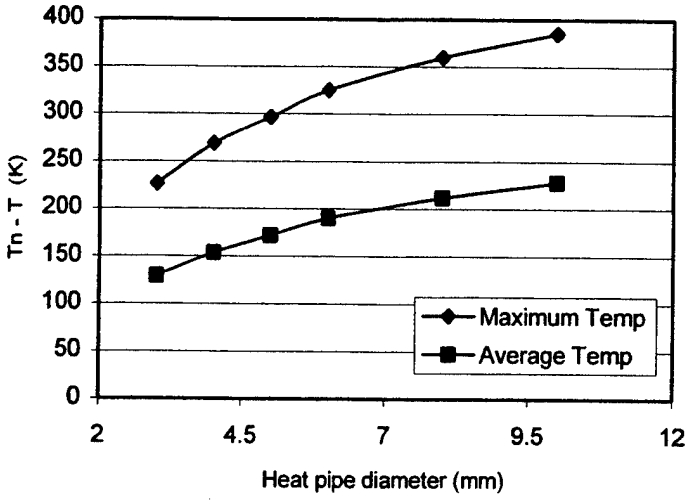

Fig. 3.2 Maximum and average temperature reductions at the disk rim surface with different heat pipe diameters (L=120 mm, k_{eff}=20,000W/m-K, cooling condition 3).

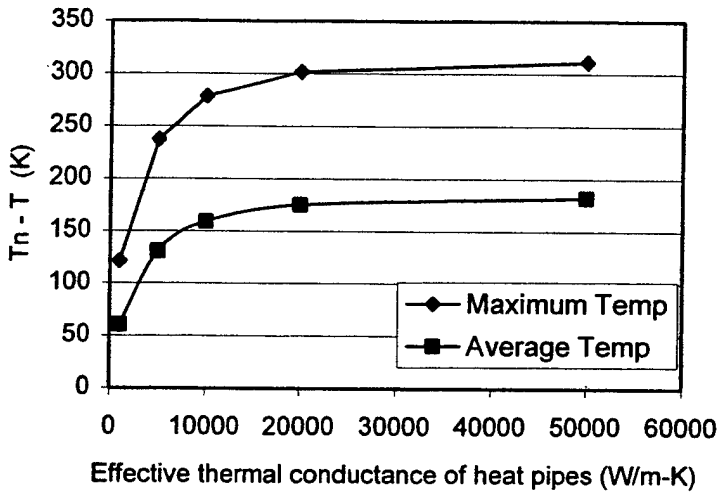

Fig. 3.3 Maximum and average temperature reductions at the disk rim and dovetail surface with different effective thermal conductance of heat pipes (di = 5 mm, L = 120 mm, cooling condition 3).

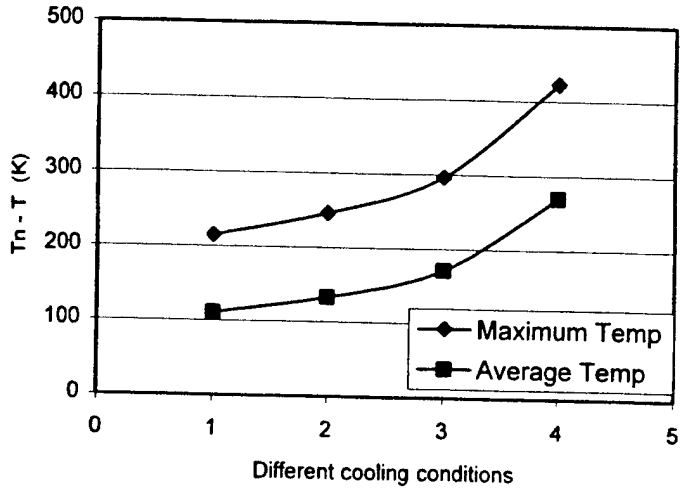

Fig. 3.4 Maximum and average temperature reductions at the disk rim and dovetail surface with different cooling conditions (d_i=5 mm, L=120 mm, k_{eff}=20,000 W/m-K),
cooling condition 1: h_2=2000 W/m-K, h_3=1400 W/m-K, h_4=600 W/m-K;
cooling condition 2: h_2=1500 W/m-K, h_3=1050 W/m-K, h_4=450 W/m-K;
cooling condition 3: h_2=1000 W/m-K, h_3=700 W/m-K, h_4=300 W/m-K;
cooling condition 4: h_2=500 W/m-K, h_3=350 W/m-K, h_4=150 W/m-K.

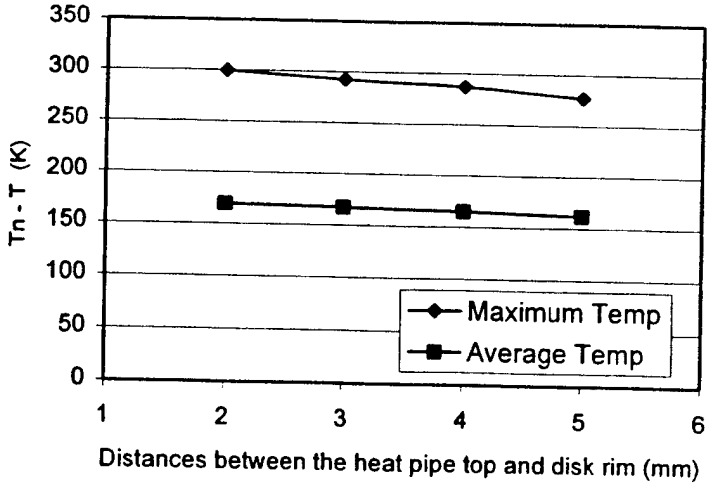

Fig. 3.5 Maximum and average temperature reductions at the disk rim and dovetail surface with different distances between the heat pipe top end and disk rim (di=5 mm, L=100 mm, cooling condition 3).

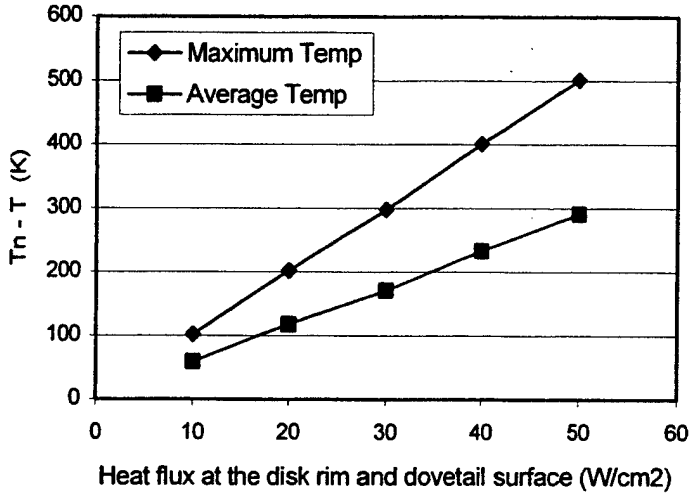

Fig. 3.6 Maximum and average temperature reductions at the disk rim and dovetail surface with different heat fluxes (di=5 mm, k_{eff}=20,000 W/m-K, L=120 mm, cooling condition 3).

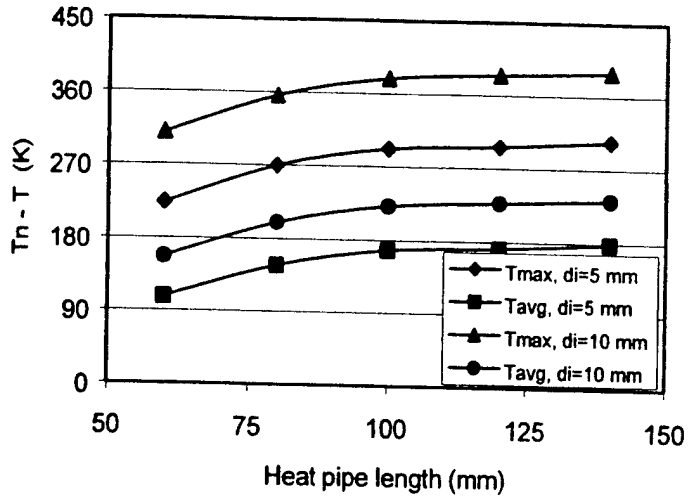

(a) temperature reductions at the disk rim and dovetail surface

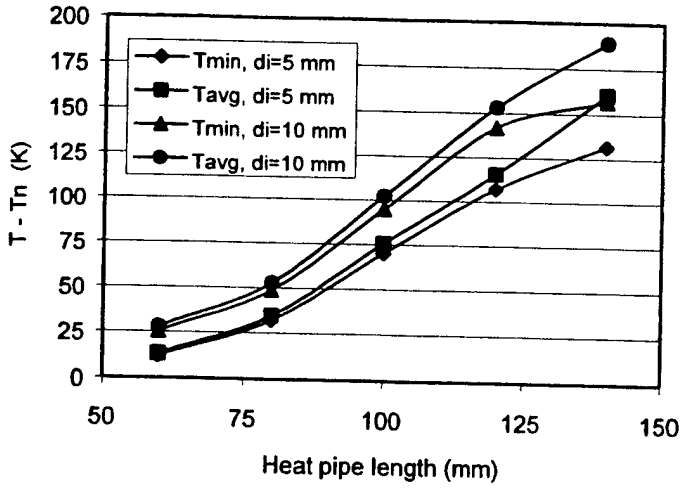

(b) temperature increase in the disk and at the disk inner surface

Fig. 3.7 Temperature reductions at the disk rim and increase at the disk inner surface W_5 (q''=30 W/cm^2, k_{eff}=20,000 W/m-K, cooling condition 3).

4. ANALYTICAL INVESTIGATIONS OF ROTATING DISKS WITH AND WITHOUT INCORPORATING ROTATING HEAT PIPES

4.1 Introduction

In section 3, comprehensive numerical analyses were presented, which provides detailed numerical results in connection with the performance of the disks incorporating radially rotating heat pipes. In this section, analytical closed-form solutions are obtained to complement the numerical results presented in section 3. The closed-form solutions have the advantages of simplicity and convenience for practical design of the heat pipe disks. An analytical closed-form solution for the disk model in Fig. 4.1 is first sought. The obtained analytical solution is then modified to accommodate the disk model in Fig. 4.2 that incorporates a number of discrete heat pipes along the circumference.

4.2 Heat Conduction Model and Analytical Solution of a Rotating Disk Having Homogeneous Properties

The model in Fig. 4.1 is a 2-D heat conduction model for a disk having homogenously thermal properties and a half-disk thickness of L. With reference to the operation of a gas turbine, intense heat from high-temperature gas and turbine blades is transferred to the disk rim surface at $r = r_2$. The two lateral surfaces of the disk are subject to strong thermal convection due to the high rotating speed of the disk, and serve as heat dissipating surfaces. The bottom surface of the half-disk shown in Fig. 4.1 is specified with an adiabatic boundary condition due to the symmetry of the structure and the temperature field. The inner surface of the disk at $r = r_1$ is approximately treated as an adiabatic surface because of a small temperature gradient there. If an excess temperature, $\theta = T - T_c$, is used, where T_c is the cooling air (ambient) temperature, the heat conduction equation and boundary conditions for the disk are as follows

$$\frac{\partial^2\theta}{\partial r^2}+\frac{1}{r}\frac{\partial\theta}{\partial r}+\frac{\partial^2\theta}{\partial z^2}=0 \qquad r_1<r<r_2 \text{ and } 0<z<L \qquad (4.1a)$$

$$\frac{\partial\theta}{\partial r}=0 \qquad \text{at } r=r_1 \qquad (4.1b)$$

$$\frac{\partial\theta}{\partial r}=\frac{q''}{k} \qquad \text{at } r=r_2 \qquad (4.1c)$$

$$\frac{\partial\theta}{\partial z}=0 \qquad \text{at } z=0 \qquad (4.1d)$$

$$\frac{\partial\theta}{\partial z}+H\theta=0 \qquad \text{at } z=L \qquad (4.1e)$$

where $H=\frac{h}{k}$. By employing the method of the separation of variables and assuming the separation of the variable θ in the form $\theta = R(r)Z(z)$, the function *R(r)* would satisfy the following equations (Arpaci, 1966; Ozisik, 1993):

$$\frac{d^2R}{dr^2}+\frac{1}{r}\frac{dR}{dr}-\eta^2R=0 \qquad r_1<r<r_2 \qquad (4.2a)$$

$$\frac{dR}{dr}=0 \qquad \text{at } r=r_1 \qquad (4.2b)$$

The solution of the above equation satisfying the boundary condition at $r = r_1$ is

$$R(\eta_m,r)=K_0'(\eta_m r_1)I_0(\eta_m r)-I_0'(\eta_m r_1)K_0(\eta_m r) \qquad (4.3)$$

Similarly, the function *Z(z)* would satisfy the following equation and boundary conditions:

$$\frac{d^2Z}{dz^2}+\eta^2Z=0 \qquad 0<z<L \qquad (4.4a)$$

$$\frac{dZ}{dz}=0 \qquad \text{at } z=0 \qquad (4.4b)$$

$$\frac{dZ}{dz} + HZ = 0 \qquad \text{at } z=L \qquad (4.4c)$$

The solution of the above differential equation satisfying the boundary conditions at z = *0* and $z = L$ is

$$Z(\eta_m, z) = \cos(\eta_m z) \qquad (4.5)$$

where the eigenvalues η_m are the positive roots of the following equation:

$$\eta_m \tan(\eta_m L) = H \qquad (4.6)$$

The complete solution of Eqs. (4.1a-4.1e) is thus constructed as

$$\theta(r,z) = \sum_{m=1}^{\infty} A_m R(\eta_m, r) Z(\eta_m, z)$$

$$= \sum_{m=1}^{\infty} A_m [K_0'(\eta_m r_1) I_0(\eta_m r) - I_0'(\eta_m r_1) K_0(\eta_m r)] \cos(\eta_m z) \qquad (4.7)$$

The unknown coefficient A_m determined by the application of the boundary condition (4.1c) and through the utilization of the orthogonality of function $Z(\eta_m, z)$ is

$$A_m = \frac{q'' \sin(\eta_m L)}{kN(\eta_m)\eta_m [K_0'(\eta_m r_1) I_0'(\eta_m r_2) - I_0'(\eta_m r_1) K_0'(\eta_m r_2)]} \qquad (4.8)$$

The normalization integral (or the norm) for this problem is

$$N(\eta_m) = \int_0^L [Z(\eta_m, z)]^2 dz = \frac{1}{2} \frac{L(\eta_m^2 + H^2) + H}{\eta_m^2 + H^2} \qquad (4.9)$$

Introducing this coefficient, A_m, into Eq. (4.7) yields

$$\theta(r,z) = \frac{q''}{k} \sum_{m=1}^{\infty} \frac{\sin(\eta_m L)}{N(\eta_m)\eta_m} \cdot \frac{K_0'(\eta_m r_1) I_0(\eta_m r) - I_0'(\eta_m r_1) K_0(\eta_m r)}{K_0'(\eta_m r_1) I_0'(\eta_m r_2) - I_0'(\eta_m r_1) K_0'(\eta_m r_2)} \cos(\eta_m z) \qquad (4.10)$$

Based on the following relations of the Bessel function,

$$I_0'(\eta_m r) = \eta_m I_1(\eta_m r) \qquad (4.11a)$$

$$K_0'(\eta_m r) = -\eta_m K_1(\eta_m r) \tag{4.11b}$$

The temperature distribution in the disk can be recast as

$$\theta(r,z) = \frac{q''}{k}\sum_{m=1}^{\infty}\frac{\sin(\eta_m L)}{N(\eta_m)\eta_m^2}\cdot\frac{K_1(\eta_m r_1)I_0(\eta_m r) + I_1(\eta_m r_1)K_0(\eta_m r)}{K_1(\eta_m r_1)I_1(\eta_m r_2) - I_1(\eta_m r_1)K_1(\eta_m r_2)}\cos(\eta_m z) \tag{4.12}$$

It is clear from Eq. (4.12) that the temperature distribution in the disk is a function of heat flux, thermal conductivity, heat transfer coefficient, and geometrical dimensions of the disk.

The same problem is also solved through a 3-D numerical calculation employing the commercial software FLUENT/GAMBIT. The number of cells, faces, and nodes used in the numerical simulation are, respectively, 32,800, 10,100, and 44,700. The discretization scheme employed is the second order upwind. The segregated solver is applied to solve the 3-D energy equation, and the residual convergence criterion is set to be 10^{-8}. It can be found from the comparison as shown in Fig. 4.4 that the analytical solution is in good agreement with the numerical calculation under the same geometry (L=*0.017* m, r_1=*0.07* m, and r_2=*0.3* m) and boundary conditions.

After the comparison between the closed-form and numerical solutions is made, the closed-form solution is employed to illustrate the effects of various parameters on the temperature distribution in the disk. The heat transfer coefficient, h, on the lateral surfaces of the turbine disk presents a strong influence on the eigenvalues η_m, norm $N(\eta_m)$, and Bessel functions $I(\eta_m r)$ and $K(\eta_m r)$ in Eq. (4.12). An increase in the heat transfer coefficient would result in an increase in the eigenvalues based on Eq. (4.6). With an increase in eigenvalues, the denominator on the right-hand side of Eq. (4.12) would rise significantly due to the term η_m^2. As a result, the temperature level in the disk

would decrease accordingly with an increase in the heat transfer coefficient. Figure 4.5 shows the temperature distributions with different heat transfer coefficients on the lateral surfaces of the disk. It can be seen from Fig. 4.5 that as the heat transfer coefficient increases from 150 to 350 W/m^2.°C, the temperature level in the disk would decrease gradually if the thermal conductivity, heat flux, and geometry of the disk are kept as constant. It should be noted from Fig. 4.5 that even at a relatively high heat transfer coefficient, the disk rim temperature is still too high. In addition, the increase of the heat transfer coefficient would require a substantial increase of the cooling-air flow rate, which would be limited by the capacity of the compressor and fuel consumption of the gas turbine engine.

It is believed that the high temperature at the disk rim is attributable to the low thermal conductivity used in the above calculation (k = 24 W/m-°C in this case). As a result, the thermal conductivity of the disk material is critical to the temperature reduction of the disk. Based on Eqs. (4.6) and (4.12), as the thermal conductivity is increased, the eigenvalues, η_m, would be reduced, and the temperature level in the disk would be decreased. At the same time, the heat transfer capability of the disk material would be increased, and the temperature distribution in the disk would become more uniform. Figure 4.6 shows temperature distributions with different thermal conductivity under the same geometry and boundary conditions. From Fig. 4.6, it is evident that as the thermal conductivity is increased from 24 to 105 W/m-°C, the temperature at the disk rim, $r = r_2$, is reduced by about 250 °C and that at the inner surface of the disk, $r = r_1$, is increased by only about 50 °C.

The size of the disk also plays an important role in determining the temperature distribution. The disk size is primarily controlled by r_2 and r_1. A larger r_2 combined with a smaller r_1 represents a larger disk while a smaller r_2 combined with a larger r_1 represents a smaller disk. Because the modified Bessel function of the first kind, I, will decrease with a decrease in r, and the modified Bessel function of the second kind, K, will increase with a decrease in r, the denominator in Eq. (4.12), $K_1(\eta_m r_1)I_1(\eta_m r_2) - I_1(\eta_m r_1)K_1(\eta_m r_2)$, will decrease when r_2 is decreased and r_1 is increased. As a result, the temperature level in the disk will rise significantly when the size of the disk is reduced (a decreased r_2 and an increased r_1). For a compact turbine design, the increase of the temperature level in the disk would be very significant if the heat load and cooling condition on the disk surfaces are kept as a constant. Figure 4.7 shows the comparison of temperature distributions with different disk sizes under the same heat flux and heat transfer coefficient. It can be seen from Fig. 4.7 that the temperature level in the entire disk could remain high if the size of the disk is small. Additionally, the disk thickness also has a significant effect on the temperature distribution in the disk. It is clear from Eq. (4.6) that the eigenvalues, η_m, would decrease with an increase in the half disk thickness, L. Accordingly, the temperature level in the disk would rise with the decrease of the term, η_m^2, in the denominator of Eq. (4.12). As a result, the disk thickness should be reduced in the design if the requirement for the disk strength can be met.

In addition to the foregoing influential parameters, it is evident from Eq. (4.12) that the temperature distribution in the disk is directly proportional to the heat flux on the disk rim. With an increase in the heat flux, the temperature in the disk will be increased

accordingly.

4.3 Modified Closed-Form Solution For a Turbine Disk Incorporating Heat Pipes

As mentioned earlier, it is believed that the major causes of a very high temperature near the disk rim are the low thermal conductivity associated with the turbine disk materials, limited cooling surface area due to a compact turbine design, and inefficiency of traditional cooling methods. The increase in the heat transfer coefficient could not necessarily produce a strong cooling effect on the disk rim if the thermal conductivity of the disk material remains low. As a result, the increase of the thermal conductivity of the disk material becomes an effective means of turbine disk cooling.

Based on this understanding, a turbine disk incorporating radially rotating heat pipes was proposed (Cao et al., 1998, 2000). Figure 4.2 schematically illustrates a proposed turbine disk incorporating a number of radially rotating heat pipes. For a practical gas turbine disk, the disk rim surface is subject to the worst heating condition, which results in the maximum temperature there. If the maximum temperature is higher than the temperature limitation that allows for a safe operation of the gas turbine disk, the disk could experience a catastrophic damage. As a result, the prediction of the maximum temperature on the disk rim is very important for the safe operation of the turbine disk.

Since Eq. (4.12) can only be applied to a disk having homogenous thermal properties and a simple geometry, such as that shown in Fig. 4.1, it must be modified before it can be used to predict the maximum temperature of a turbine disk incorporating heat pipes, which is shown in Fig. 4.2. In the remainder of this section, a modification correlation that takes into account the heat pipe geometry/location and thermal conductance is established with the assistance of numerical calculations. To establish the

framework of the correlation, the important parameters that need to be included in the correlation are briefly discussed. The distance between the heat pipe top and the disk rim surface, s, is important for the determination of the maximum temperature. A small s would enhance the heat transfer from the disk rim to the heat pipe so that the maximum temperature at the disk rim surface could be reduced. However, the distance could not be too small because of the concern of mechanical strength at the disk rim. The heat pipe length, L_{hp}, also has a significant influence on the maximum temperature on the disk rim surface. With an increase in heat pipe length, more heat from the disk rim can be carried to the inner lower-temperature region so that the cooling effect at the lateral surfaces of the disk would be enhanced and the maximum temperature at the disk rim would be reduced. These two parameters, s and L_{hp}, can be combined into a dimensionless number, $(\frac{s}{L_{hp}})$. This dimensionless number can be included in the correlation to represent the influence of both s and L_{hp} on the maximum temperature at the disk rim.

Since the heat pipes are incorporated in the disk to increase the effective thermal conductivity of the disk, the thermal conductivity, k, of the disk material in Eq. (4.12) should be replaced by an average or effective thermal conductivity, k_a, which includes the influence of both the disk material thermal conductivity and heat pipe thermal conductance.

$$k_a = k(1 - \frac{A_{hp}}{A_a}) + k_{eff} \frac{A_{hp}}{A_a} \tag{4.13}$$

where $A_{hp} = n\pi r_{hp}^2$ and $A_a = 2\pi r_a L$. A_{hp} is the total cross-sectional area of the heat pipes incorporated, n is the number of heat pipes incorporated in the disk. r_a is the average radius of the disk, $r_a = (r_1+r_2)/2$, and A_a is the sectional area of the disk at the average

radius, r_a. In addition to the thermal conductivity, the heat transfer coefficient, h, would also influence the maximum temperature at the disk rim. As a result, another dimensionless parameter, $(\frac{k}{hr_2})$, is introduced and is included in the correlation to reflect the effect of both thermal conductivity and heat transfer coefficient.

Having introduced the foregoing two dimensionless numbers, the ratio of the temperature distribution at the disk rim incorporating the heat pipes to that from Eq. (4.12) can be expressed by the following equation:

$$\frac{\theta_{\max}(r_2,z)}{\theta(r_2,z)} = c_1(\frac{s}{L_{hp}})^{C_2}(\frac{k}{hr_2})^{C_3} \tag{4.14}$$

In general, the maximum temperature at the disk rim surface occurs at z = 0. Therefore, the modified closed-form solution for the maximum temperature at the disk rim can be rewritten as the following:

$$\frac{\theta_{\max}(r_2,0)}{\theta(r_2,0)} = c_1(\frac{s}{L_{hp}})^{C_2}(\frac{k}{hr_2})^{C_3} \tag{4.15}$$

where $\theta(r_2,0) = \frac{q''}{k_a}\sum_{m=1}^{\infty}\frac{\sin(\eta_m L)}{N(\eta_m)\eta_m^2}\cdot\frac{K_1(\eta_m r_1)I_0(\eta_m r_2)+I_1(\eta_m r_1)K_0(\eta_m r_2)}{K_1(\eta_m r_1)I_1(\eta_m r_2)-I_1(\eta_m r_1)K_1(\eta_m r_2)}$. C_1, C_2 and C_3 are constants to be determined.

4.4 Determination of the Constants in the Correlation Employing Numerical Results

In section 4.3, the modification correlation for the maximum temperature at the disk rim incorporating the heat pipe has been derived. However, the constants, C_1, C_2 and C_3, in the correlation should be determined. In this section, extensive 3D numerical

calculations are made and the resulting numerical results are used for the determination of these three constants.

Because of the structural symmetry, only a disk sector containing two halves of the heat pipes is numerically modeled, as shown in Fig. 4.3. To simplify the analysis, the heat pipes installed in the disk are treated as solid bars having a high effective thermal conductance, k_{eff}. This simplification is the same as that adopted by Cao et al. (2000) and could avoid solving the complicated two-phase flow in the heat pipe. Due to the structural concern, a distance, s, is maintained between the heat pipe top end and disk rim surface, as shown in Fig. 4.3.

Because the radiation heat transfer rate at the disk surface is much smaller than the convection heat transfer rate, it is neglected in the numerical simulation. Numerical simulations are made by employing the commercially available computer software FLUENT. The disk and heat pipes are meshed into hexahedral cells. The total number of cells is about 26,000, and the convergent criterion is 10^{-8}. During the simulations, parameters in connection with heat input, air cooling condition, material properties, disk geometry, and heat pipe dimensions are varied within the following ranges:

$10^5 W/m^2 \le q'' \le 5\times10^5 W/m^2$; $k_{eff} = 10{,}000\, W/m^2.^oC$; $k = 24 W/m.^oC$;

$3mm \le s \le 20mm$; $T_c = 525^oC = 798K$; $0.04m \le L_{hp} \le 0.2m$; $1.5mm \le r_{hp} \le 3.5mm$;

$100 W/m^2.^oC \le h \le 500 W/m^2.^oC$; $0.07m \le r_1 \le 0.1m$; $0.25m \le r_2 \le 0.5m$; $L=0.017\ m$.

where L_{hp} is the heat pipe length, T_c is the cooling air temperature which is set as a constant to simplify the numerical simulation, r_1 and r_2 are inner and outer radii of the disk, and r_{hp} is the heat pipe radius.

A large number of numerical data are generated through the numerical simulation and are employed to determine the three constants, C_1, C_2 and C_3, in the correlation through a multivariable regression analysis. Three constants thus determined are as follows:

$$C_1=1.66, \quad C_2=0.03, \quad C_3=-0.37$$

Substituting all these constants into Eq. (4.15), a modified closed-form solution for the maximum temperature at the disk rim incorporating the heat pipe is obtained:

$$\frac{\theta_{mas}(r_2,0)}{\theta(r_2,0)} = 1.66\left(\frac{s}{L_{hp}}\right)^{0.03}\left(\frac{k}{hr_2}\right)^{-0.37} \tag{4.16a}$$

The above equation can be recast as

$$\theta_{\max}(r_2,0) = 1.66\left(\frac{s}{L_{hp}}\right)^{0.03}\left(\frac{k}{hr_2}\right)^{-0.37}\frac{q^{"}}{k_a}\sum_{m=1}^{\infty}\frac{\sin(\eta_m L)}{N(\eta_m)\eta_m^2}\cdot\frac{K_1(\eta_m r_1)I_0(\eta_m r_2)+I_1(\eta_m r_1)K_0(\eta_m r_2)}{K_1(\eta_m r_1)I_1(\eta_m r_2)-I_1(\eta_m r_1)K_1(\eta_m r_2)} \tag{4.16b}$$

The ranges of the two dimensionless parameters and average thermal conductivity corresponding to the numerical data used are

$$0.025 \le \frac{s}{L_{hp}} \le 0.125,\ 0.096 \le \frac{k}{hr_2} \le 0.96, \text{ and } 160 W/m^2.^oC \le k_a \le 763 W/m^2.^oC.$$

The modified closed-form solution for the maximum temperature at the disk rim, Eq. (4.16), is compared with the corresponding numerical results in Fig. 4.8. Apparently, Eq. (4.16) is in good agreement with the numerical results, and all numerical data fall within 10% of Eq. (4.16). As a result, Eq. (4.16) can be used within the uncertainty range to predict the maximum temperature at the disk rim incorporating radially rotating heat pipes. The deviation between Eq. (16) and the numerical results may be attributable to the errors in connection with numerical simulation, calculating errors from Eq. (4.16), which

include the errors of the Bessel functions and truncation errors of the infinite serials, and the errors associated with the mathematical formulation of Eq. (4.16).

4.5 Conclusions

The closed-form solution for a rotating disk having homogenous thermal properties is derived. The analytical solution is then used to illustrate the effects of various parameters on the temperature distribution in the disk. To accommodate the disk incorporating the heat pipe, the closed-form solution is modified through a modification correlation. The correlation is subsequently established using numerical data from extensive 3D numerical simulation. The modified closed-form solution thus obtained is compared with corresponding numerical data in good agreement. In summary, the closed-form solutions generated through this study can provide a useful and convenient tool for simulating the performance of a turbine disk with and without incorporating the heat pipe.

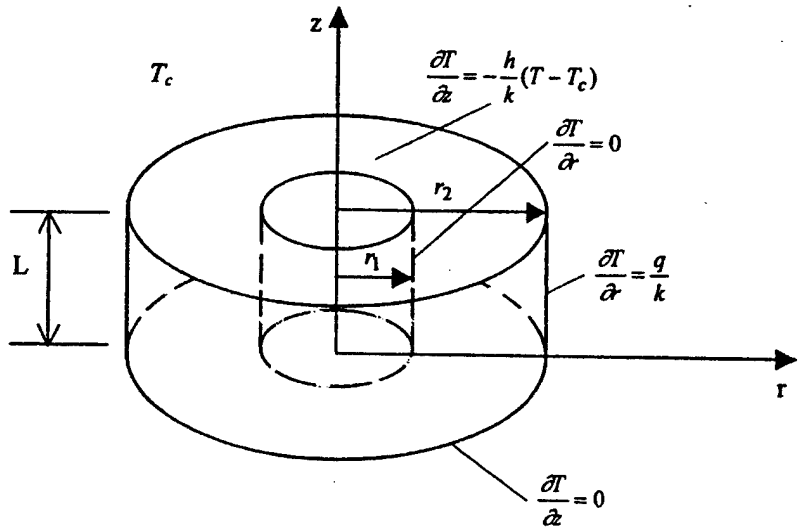

Fig. 4.1 Schematic of a rotating disk under a cylindrical coordinate system.

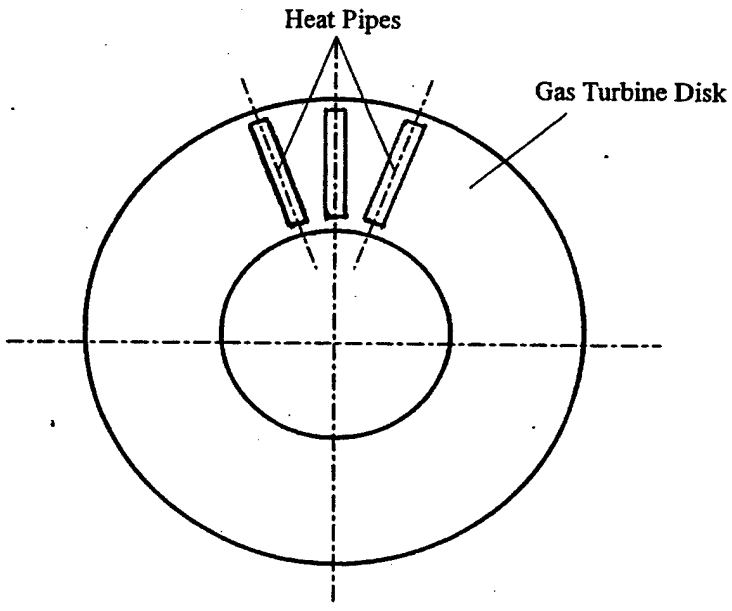

Fig. 4.2 Schematic of a turbine disk incorporating radially rotating heat pipes.

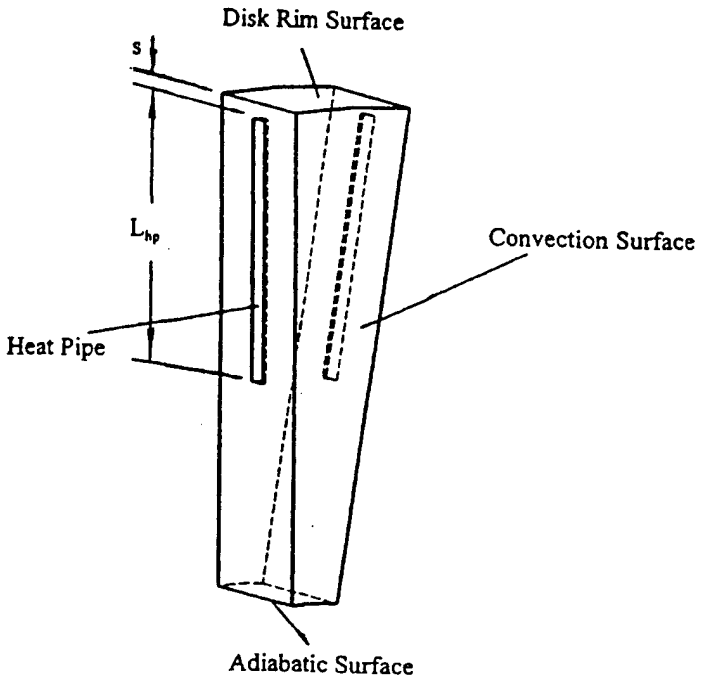

Fig. 4.3 Schematic of a sector of simulated turbine disk with radially rotating heat pipes.

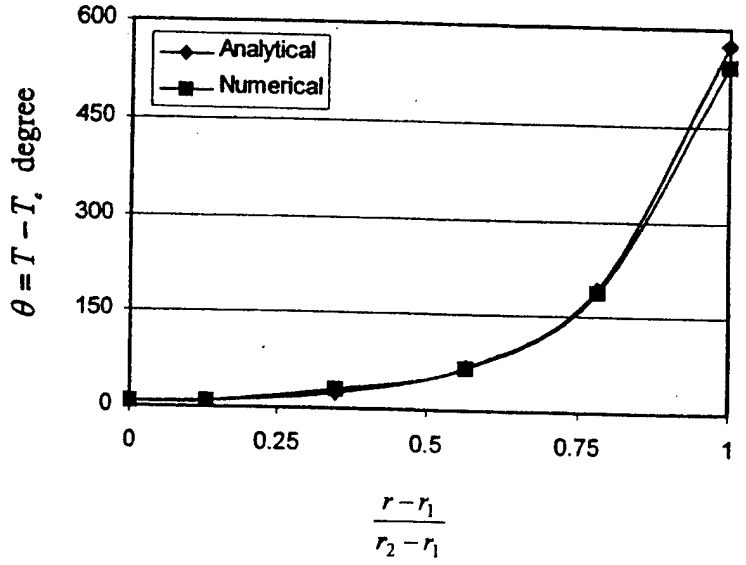

Fig. 4.4 Comparison of the analytical and numerical solutions under the same geometry and boundary conditions (h=250 W/m².°C, q''=3×10^5 W/m², z=0, k=24 W/m-°C, and T_c =525 °C).

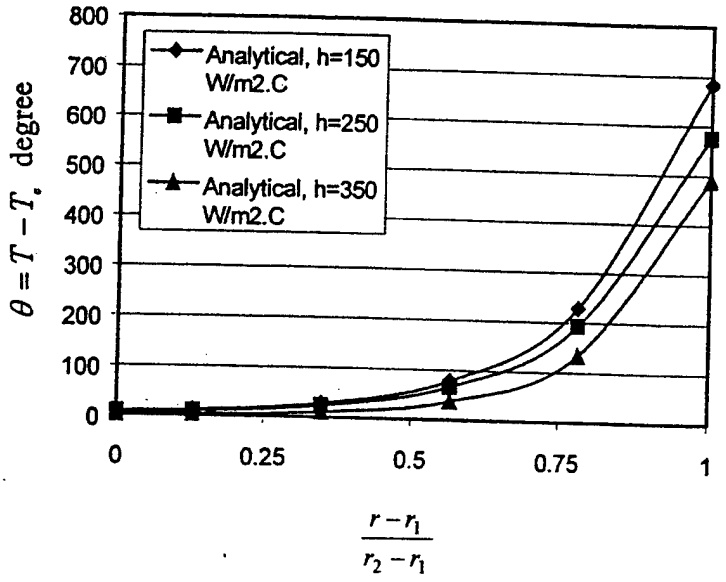

Fig. 4.5 Comparison of the temperature distributions with different heat transfer coefficients under the same geometry and boundary conditions ($q''=3\times10^5$ W/m², $z=0$, $k=24$ W/m-°C, and $T_c=525$ °C).

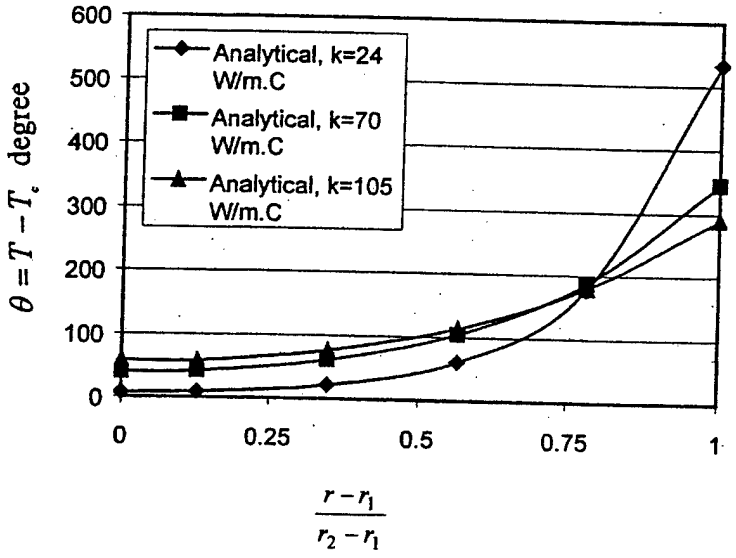

Fig. 4.6 Comparison of the temperature distributions with different thermal conductivity under the same geometry and boundary conditions ($h=250$ W/m².°C, $q''=3\times10^5$ W/m², $z=0$, and $T_c=525$ °C).

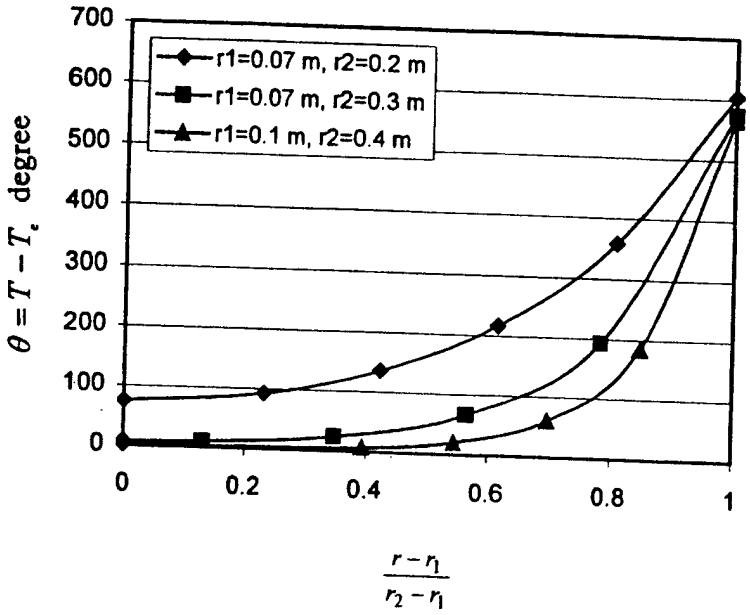

Fig. 4.7 Comparison of the temperature distributions with different outer radii ($q''=3\times10^5$ W/m², k=24 W/m-°C, $h=250$ W/m².°C, $z=0$, $T_c=525$ °C).

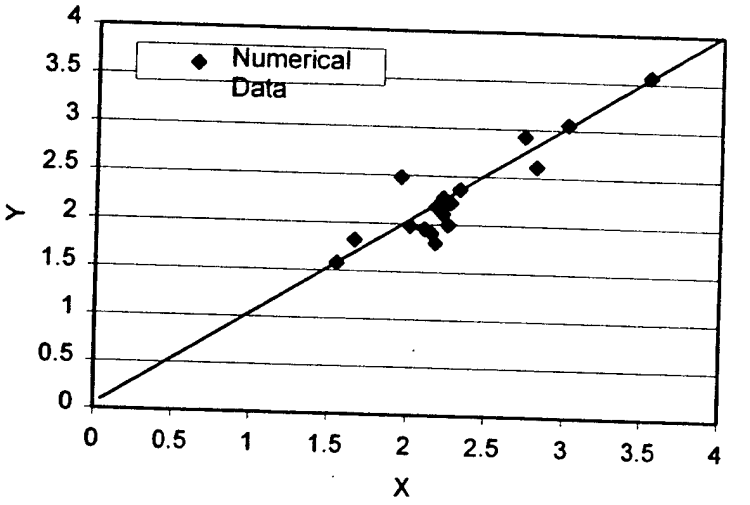

where $Y=\dfrac{\theta_{\max}(r_2,0)}{\theta(r_2,0)}$, $X=1.66(\dfrac{s}{L_{hp}})^{0.03}(\dfrac{k}{hr})^{-0.37}$

Fig. 4.8 Comparison of the closed-form analytical solution and numerical data for the maximum disk temperatures under the different conditions.

5. NUMERICAL INVESTIGATIONS OF A GAS TURBINE DISK-BLADE ASSEMBLY INCORPORATING RADIALLY ROTATING HEAT PIPES

5.1 Introduction

Through the research work in the previous sections, the feasibility of incorporating wickless radially rotating heat pipes into a turbine disk for the reduction of disk rim temperature has been proven. In general, a temperature reduction of 150-250°C at the disk rim is achievable through this technique. It is anticipated that the turbine blades attached to the disk rim would work at a lower temperature under the same air-cooling condition when the disk rim temperature is substantially reduced. However, this enhanced cooling effect on the turbine blades has not been studied. Comprehensive numerical simulation will be performed for a high-pressure turbine stage that incorporates rotating heat pipes in the disk and employs the state-of-the-art air cooling technique for the turbine blade. The results will be compared with those of a turbine stage employing the air cooling technique for the turbine blade alone. Various parameters that could affect the temperature reduction of the turbine blades will be examined and the net benefit of turbine blade cooling will be evaluated at the turbine stage system level.

In the current numerical simulation, both turbine disk and turbine blades will be included. In the turbine disk, like the case in the previous study, heat pipes are embedded. A built-in channel is provided in the disk to supply the cooling air to the blade cooling system. Both the heat pipe and the flow channel can have the function of reducing the high temperature in the disk. The cooling system in the blade includes a number of cooling channels built inside the blade. The disk and blade are assembled with the blade root attached to the disk near the disk rim. Unlike the previous study in which

the turbine disk was studied alone, no heat flux boundary conditions are needed at the disk rim. Instead, the turbine disk and the turbine blade will be solved simultaneously in conjunction with the cooling air on the side surfaces of the disk, the cooling air flow within the cooling channel of the blade, and the heat transfer from the mainstream combustion gas to the blade. In the current study, the cooling air flow within the blade and the disk rim is intended to be solved as a field problem, i.e., only the inlet condition of the cooling air is specified, and the turbine blade/disk and the cooling air will be solved as a conjugate problem. For the heat transfer between the mainstream combustion gas and the blade, appropriate heat transfer coefficients will be specified. Through this treatment, the complexity of the problem can be reduced to a certain extent and the accuracy of the solution can be maintained.

5.2 Numerical Modeling

Because of the structural symmetry, only a disk-blade assembly sector is numerically modeled. Fig. 5.1 shows schematically disk-blade assembly sector of a conventional reference disk without heat pipes and Fig. 5.2 illustrates a disk-blade assembly sector of the same size incorporating radially rotating heat pipes. As shown in Figs. 5.1 and 5.2, the cooling air from the compressor flows into the disk from the cooling air inlet and passes through the internal cooling passage of the blade. Finally, the cooling air is discharged from the cooling air outlet on the top of the blade. At the same time, two lateral sides of the disk are subject to the cooling from the cooling air. As a result, the disk-blade assembly is subject to turbulent convection heat transfer in the cooling air passage and heat conduction in the disk-blade assembly materials. Due to the symmetry of the disk-blade assembly sector, only two halves of the heat pipes are shown

in Fig. 5.2. To simplify the numerical analysis, the rotating heat pipes in Fig. 5.2 are treated as a solid cylinder with an effective thermal conductance, k_{hp}, to avoid solving the complicated two-phase flow in the heat pipes.

The governing equation for the three-dimensional heat conduction in a solid is:

$$\frac{\partial}{\partial t}(\rho h) = \frac{\partial}{\partial x_i}(k\frac{\partial T}{\partial x_i}) \qquad \text{i} = 1, 2, 3 \qquad (5.1)$$

where h is the specific enthalpy and $T = f(\vec{r}, t)$. The thermal conductivity in the above equation should be replaced by the effective thermal conductance, k_{hp}, in the heat pipe regions. The general boundary condition for the heat transfer can be represented by the following equation:

$$\frac{\partial T}{\partial x_i} = f_i(\vec{r}, t) \qquad (5.2)$$

where $f(\vec{r}, t)$ is a function of the position vector and time. The heat transfer rate at a surface is attributable to the convection, and can be represented by the following relation:

$$q_i'' = h_i \Delta T \qquad (5.3)$$

The governing equations for the three-dimensional convection heat transfer in the cooling air passage are as follows:

Mass conservation equation:

$$\frac{\partial u_i}{\partial x_i} = 0 \qquad (5.4)$$

Momentum equation:

$$\frac{\partial}{\partial x_j}[(\mu_l + \mu_t)(\frac{\partial u_i}{\partial x_j} + \frac{\partial u_j}{\partial x_i} - \delta_{ij}\frac{2}{3}\frac{\partial u_k}{\partial x_k}) - \rho u_j u_i - \delta_{ij} p] = 0 \qquad (5.5)$$

Energy equation:

$$\frac{\partial}{\partial x_j}[(\frac{\mu_t C_p}{\sigma_T})\frac{\partial T}{\partial x_j} - \rho u_j C_p T] + \mu_t \Phi_v + \rho\varepsilon = 0 \tag{5.6}$$

The turbulent kinetic energy in the $k-\varepsilon$ turbulent model:

$$\frac{\partial}{\partial x_j}[(\mu_l + \frac{\mu_t}{\sigma_k})\frac{\partial k}{\partial x_j} - \rho u_j k] + \rho P - \rho\varepsilon = 0 \tag{5.7}$$

Dissipation rate of the turbulent kinetic energy:

$$\frac{\partial}{\partial x_j}[(\mu_l + \frac{\mu_t}{\sigma_\varepsilon})\frac{\partial \varepsilon}{\partial x_j} - \rho_f u_{f,i}\varepsilon] + C_{\varepsilon 1}\frac{\rho_f \varepsilon P}{k} - C_{\varepsilon 2}\frac{\rho\varepsilon^2}{k} = 0 \tag{5.8}$$

where $P = \frac{\mu_t}{\rho_f}\frac{\partial u_i}{\partial x_j}(\frac{\partial u_i}{\partial x_j} + \frac{\partial u_j}{\partial x_i})$, (5.9)

$$\Phi_v = \frac{\partial u_i}{\partial x_j}(\frac{\partial u_i}{\partial x_j} + \frac{\partial u_j}{\partial x_i} - \frac{2}{3}\frac{\partial u_k}{\partial x_k}\delta_{ij}), \tag{5.10}$$

μ_t is the turbulent viscosity, which is computed from the relation: $\mu_t = \rho_f C_\mu k^2/\varepsilon$, and all empirical constants for the $k-\varepsilon$ turbulent model are as follows:

C_μ=0.09, $C_{\varepsilon 1}$=1.44, $C_{\varepsilon 2}$=1.92, σ_T=0.7, σ_k=1.0, σ_ε=1.3.

A non-slip boundary condition is imposed on the walls. Moreover, in the near-wall zone, the standard wall function was chosen for this study due to its wide application in industrial fluid flows. When the mesh is such that $y^* \le 11.225$ at the wall-adjacent cells, the viscous force is dominant in the sublayer. The laminar stress-strain relationship can be applied

$$u^* = y^* \tag{5.11}$$

$$y^* = \frac{\rho_m C_\mu^{\frac{1}{4}} k_p^{\frac{1}{2}} y_p}{\mu_m} \tag{5.12}$$

The logarithmic law for the mean velocity is known to be valid for $y^* > 11.225$ (Fluent Inc., 1996), which can be expressed as

$$u^* = \frac{1}{k}\ln(Ey^*) \tag{5.13}$$

where ρ_m and μ_m are density and viscosity, k is the von Karman's constant, C_μ is turbulent model constant, k_p and y_p are the turbulent kinetic energy at point p and the distance from point p to the wall, respectively. To simplify the simulation, the pressure inlet and outlet boundary conditions are imposed on the cooling air inlet and outlet.

In the simulation, various parameters in connection with the disk/blade configuration, thermal properties, and cooling conditions are specified as the follows:

Disk diameter: 0.6 m; Shaft diameter: 0.2 m; Disk thickness: 0.025 m; Airfoil length: 0.08 m; Diameter of cooling air inlet: 0.005 m; The number of blades in a disk: 60; Thermal conductivity of disk-blade assembly material, *k*: 24 *W/m-K*; Gas temperature, T_{gas}: 1700 *K*; Heat transfer coefficient on the blade airfoil surface and disk rim: 250 $W/m^2.K$; Heat transfer coefficient on the lateral sides of the disk: 150 $W/m^2.K$; The temperature range of the cooling: 523 K - 798 K; Flow rate of cooling air: 0.000228 *kg/s*; The range of effective thermal conductance in the rotating heat pipes in this report: 10,000 to 50,000 *W/m-K*; The range of heat pipe lengths: 0.06 - 0.12 *m*; The range of heat pipe diameters: 0.004 to 0.01 *m*; The range of distance between the disk rim and heat pipe top, *s*: 0.003 *m* to 0.005 *m*.

An unstructured grid system with tetrahedral cells was used to mash the computation domain. The numbers of cells in the cooling air passage and disk-blade

assembly are about 6,835 to 110,000, respectively, and the number of cells in the half heat pipe is from 1,000 to 4,400.

In the numerical investigation, all governing equations in conjunction with the wall boundary conditions and the inlet and outlet boundary conditions were solved in a Cartesian coordinate system by employing the CFD solver, FLUENT 6, based on a control volume finite difference method (CVFDM). SIMPLEC algorithm was used to resolve the coupling between the velocity and pressure. The second order upwind was selected to assure a better discretization accuracy. To accelerate the convergence, the under-relaxation technique was applied in all dependent variables. A segregated solver was adopted to solve the governing equations sequentially. Using SIMPLE-Partial Elimination Algorithm, the variables for each phase were eliminated from the momentum equations for all other phases. The numerical computation was considered converged when the residual summed over all the computational nodes at n^{th} iteration, R_ϕ^n, satisfied the following criterion:

$$\frac{R_\phi^n}{R_\phi^m} \leq 10^{-4} \tag{5.14}$$

where R_ϕ^m is the maximum residual value of ϕ variable after m iterations.

5.3 Results and Discussions

Figures 5.3 illustrates the temperature distribution in a disk-blade assembly without heat pipes with a cooling air temperature of 798 K. The cooling air flows into the blade cooling passage from the cooling air inlet in the disk and is discharged from the cooling air outlet on the blade tip. In Fig. 5.3, the dark red at the blade airfoil represents the highest temperature, and dark blue in the disk represents the lowest temperature. The

green represents the temperatures between the highest and lowest temperature. As shown in Fig. 5.3, the average temperature on the airfoil is 1,556 K, the average temperature at disk rim is 1147 K, and the average temperature at the disk base is 810 K.

Figure 5.4 illustrates the temperature distribution in a disk-blade assembly incorporating heat pipes with the same cooling and heating boundary conditions and disk-blade assembly dimensions as those in Fig. 5.3. It is clear that due to the heat transfer function of the heat pipes, the green at the disk rim has faded evidently, and the temperature distribution at the disk rim is decreased. Because the heat pipe has a very high thermal conductance, more heat at the disk rim is transferred to the middle part of the disk where heat is carried away by the cooling air, which results in a lower temperature distribution at the disk rim.

Figure 5.5 shows the average, maximum, and minimum temperature reductions between the proposed disk and the conventional disk under the same cooling and heating conditions, where $L_{hp}/\Delta L$ is the dimensionless heat pipe length, L_{hp} is the heat pipe length, and ΔL is defined as the difference between the disk radius and shaft radius, which is 0.2 m in this case. The cooling air temperature was taken to be 798 K in the calculations. It can be seen from Fig.5.5 that as the dimensionless heat pipe length is increased, the average, maximum, and minimum temperature reductions are increased. It indicates that a larger dimensionless heat pipe length will result in a better cooling effect and lower temperature distribution at the disk rim. The average rim temperature reduction can approach more than 100 degree when the dimensionless length is more than 0.4.

Figure 5.6 shows the average temperature reduction at the airfoil surface and average temperature increase at the disk base. The cooling and heating conditions are the

same as those for the results in Fig. 5.5. It is evident that the average temperature reduction at the airfoil surface is not sensitive with the dimensionless heat pipe length, which is less than 15 degree. But the average temperature increase at the disk base will be up to 40 degree as the dimensionless heat pipe length reaches 0.6. Because the heat at the disk rim is transferred to the location closer to the disk base by the heat pipes as the dimensionless heat pipe length is increased, the temperature at the disk base will be increased accordingly.

Figure 5.7 presents the average, maximum and minimum temperature reductions at the disk rim with different dimensionless heat pipe diameters, d_{hp}/b, where the distance from the heat pipe top to the disk rim surface, s, is 0.003 m, the heat pipe length, L_{hp}, is 0.08 m, the disk thickness, b, is 0.025 m, and the effective thermal conductance, h_{hp}, is 20,000 $W/m^2.K$. It can be seen from Fig. 5.7 that all temperature reductions at the disk rim will be increased as the dimensionless heat pipe diameter is increased. Therefore, the dimensionless heat pipe diameter should be relatively large if the material strength requirement for the disk is met.

Figure 5.8 shows the average, maximum and minimum temperature reductions at the disk rim with different cooling air temperatures, where d_{hp}= 0.008 m,, L_{hp}= 0.1 m, h_{hp}= 20,000 $W/m^2.K$, and s =0.003 m. The range of cooling air temperature is from 523 K to 798 K. As shown in Fig. 5.8, the cooling air temperature plays an important role in the cooling of a disk incorporating heat pipes. As the cooling air temperature is lowered, all temperature reduction at the disk rim are increased and the cooling effect at the disk rim is improved. It means that a lower cooling air temperature will result in a better cooling effect at the disk rim.

Figure 5.9 presents the average and maximum temperature reductions at the disk rim and average temperature reduction at the airfoil surface as the effective thermal conductance of the heat pipes is changed, when d_{hp} = 0.008 m, L_{hp} =0.1 m. and T_c = 798 K. The temperature reductions at the disk rim are increased evidently as the effective thermal conductance of the heat pipes is increased from 5,000 to 20,000 W/m^2-K. Then the temperature reduction at the disk rim is almost invariant as the effective thermal conductance of the heat pipes is increased from 20,000 to 30,000 W/m^2-K. This indicates that the heat pipe with a moderate effective thermal conductance can work very well in the proposed disk-blade assembly incorporating heat pipes. The thermal conductance of 20,000 $W/m^2.K$ is equal to 51.8 times the thermal conductivity of copper. According to the experiments presented in section 2, the effective thermal conductance of the radially rotating heat pipes is 60-100 times higher than the thermal conductivity of copper. As a result, the proposed disk-blade assembly incorporating radially rotating heat pipes should be feasible.

Figure 5.10 shows the average and maximum temperature reductions at the disk rim and average temperature reduction at the airfoil surface as the distance between the disk rim and heat pipe top, s, is changed, when d_{hp} = 0.008 m, L_{hp} = 0.1 m, h_{hp} = 20,000 W/m^2-K, and T_c = 798 K. As shown in Fig. 10, the temperature reductions at the disk rim is gradually decreased, but the average temperature reduction at the airfoil surface is almost invariant as the distance between the disk rim and the heat pipe top is increased.

5.4 Conclusions

Based on the foregoing numerical investigations, the following conclusions may be made:

1. The disk cooling technology incorporating radially rotating heat pipes is feasible. It can reduce the temperature distribution at the disk rim effectively. The magnitude of the temperature reduction at the disk rim could be further increased when a larger value of the heat transfer coefficient at the blade surface is used in the numerical calculation.
2. Both heat pipe length and heat pipe diameter have an important effect on the proposed disk cooling technology. A longer or larger heat pipe will have a better cooling effect, which results in a lower temperature distribution at the disk rim. In addition, a lower cooling air temperature will result in a bigger temperature reduction at the proposed disk-blade assembly.
3. The disk cooling technology incorporating radially rotating heat pipes has a limited effect on the maximum and average temperatures at the airfoil surface. These temperatures are mainly controlled by the cooling and heating conditions at the blades. One of the possible causes could be that the heat pipe is not used in the turbine blade. However, it is unclear at this point that the use of the heat pipe in the turbine blade would significantly reduce the blade temperature in conjunction with the use of the heat pipe in the turbine disk.

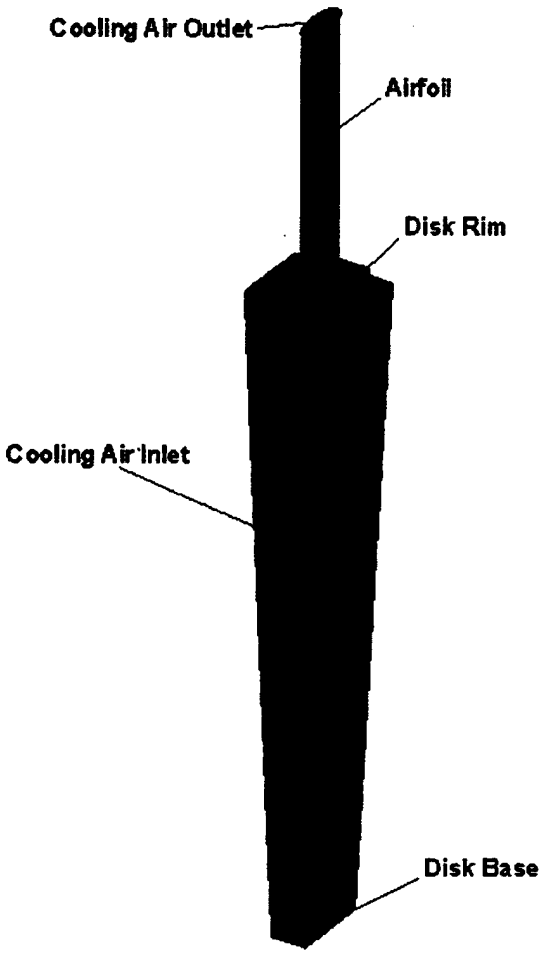

Fig. 5.1 Schematic of a disk-blade assembly.

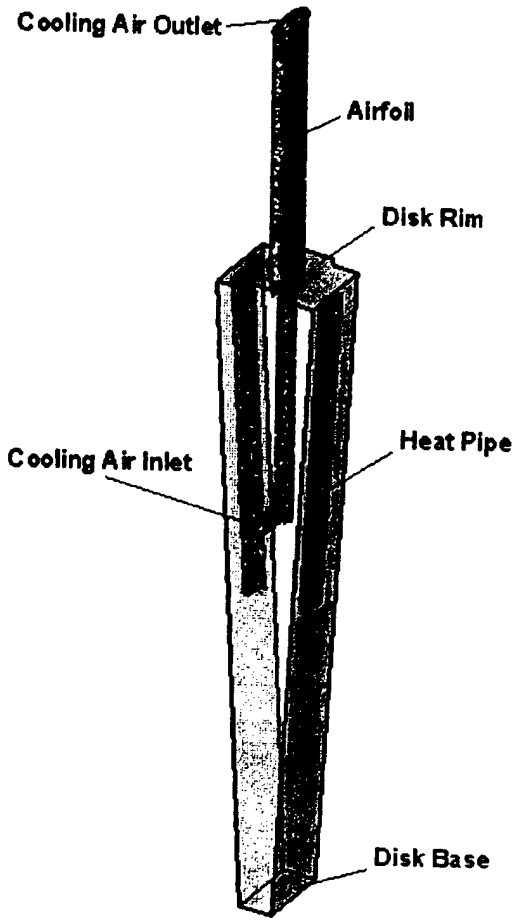

Fig. 5.2 Schematic of the disk-blade assembly incorporating heat pipes.

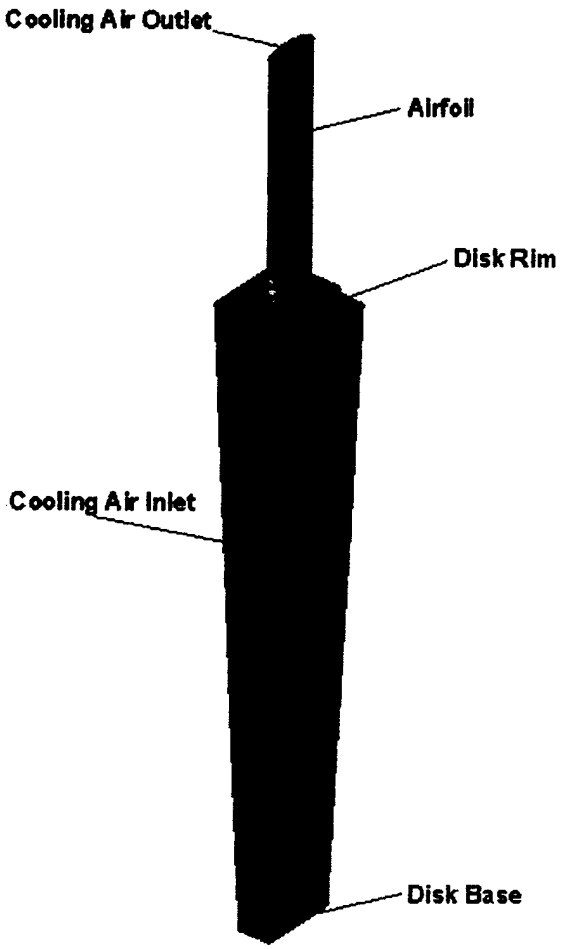

Fig. 5.3 Temperature distribution in the disk-blade assembly.

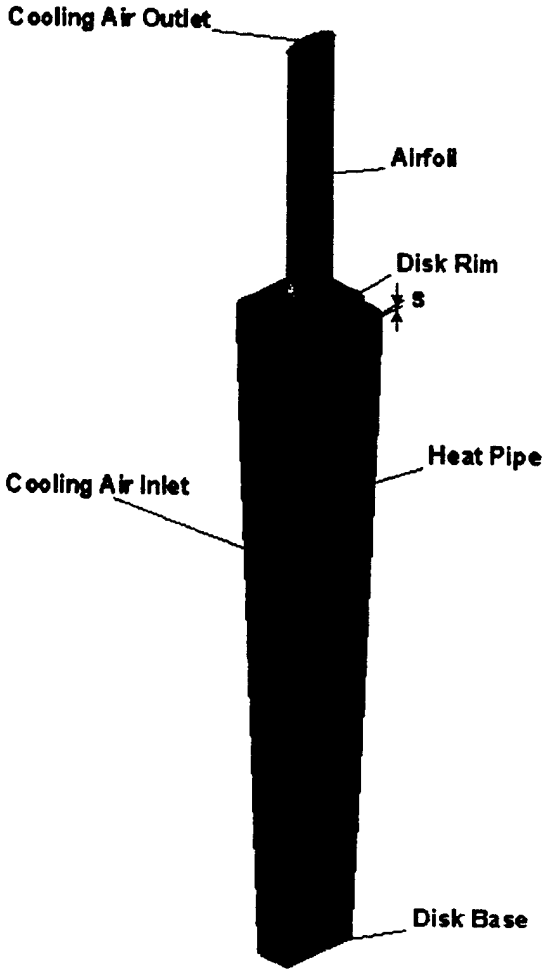

Fig. 5.4 Temperature distribution in the disk-blade assembly incorporating heat pipes.

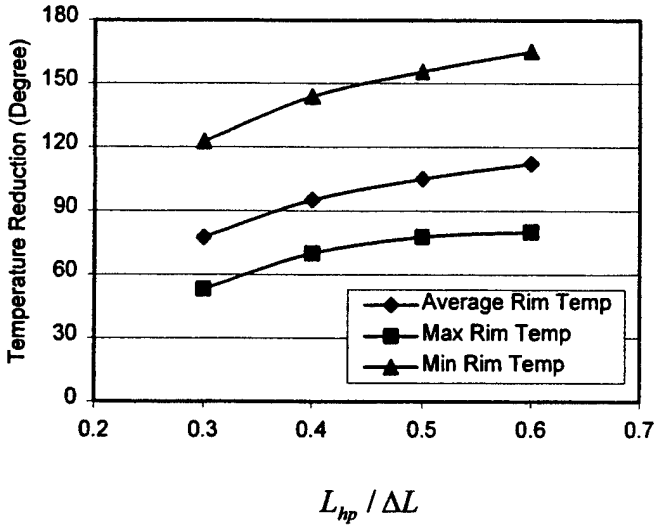

Fig. 5.5 Average, maximum and minimum temperature reduction at the disk rim with different dimensionless heat pipe lengths (s =0.003 m, d_{hp}=0.008 m, h_{hp}=20,000 $W/m^2.K$).

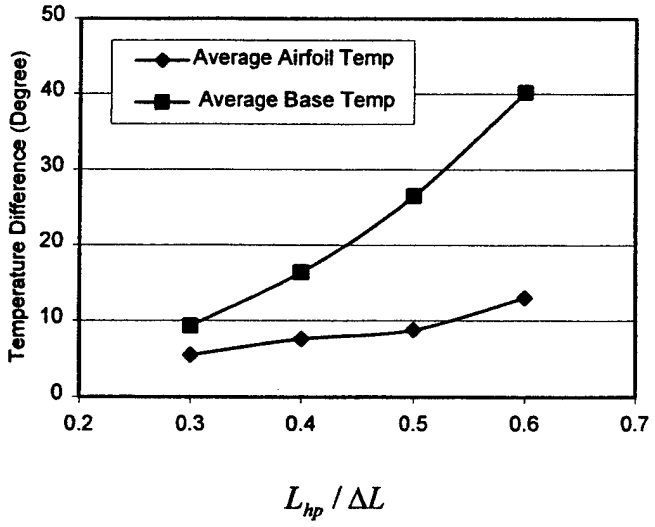

Fig. 5.6 Average temperature reduction at the airfoil surface and average temperature increase at the disk base with different dimensionless heat pipe lengths (s =0.003 m, d_{hp}=0.008 m, h_{hp}=20,000 $W/m^2.K$).

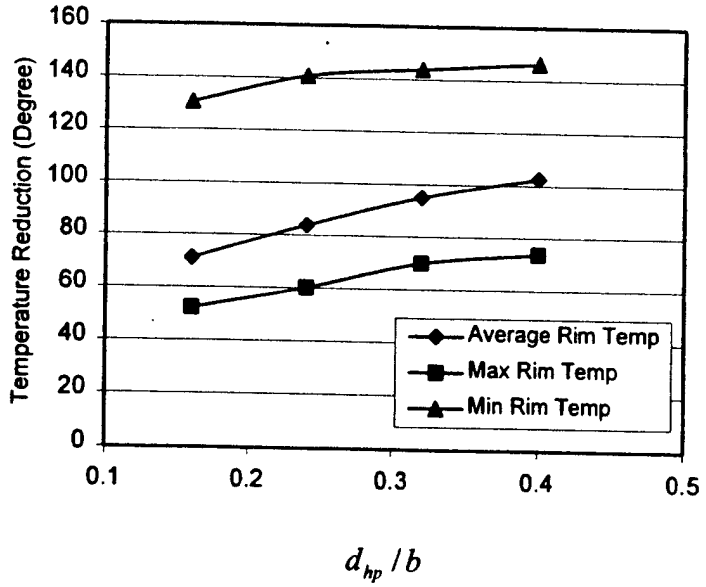

Fig. 5.7 Average, maximum and minimum temperature reductions at the disk rim with different dimensionless heat pipe diameters (s =0.003 m, L_{hp}=0.08 m h_{hp}=20,000 $W/m^2.K$).

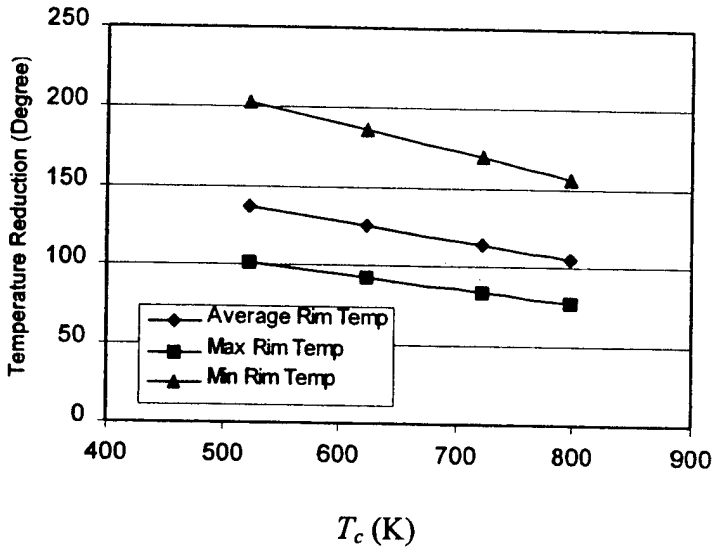

Fig. 5.8 Average, maximum and minimum temperature reductions at the disk rim with different cooling air temperatures (d_{hp} =0.008 m, h_{hp} =20,000 $W/m^2.K$, L_{hp}=0.1 m).

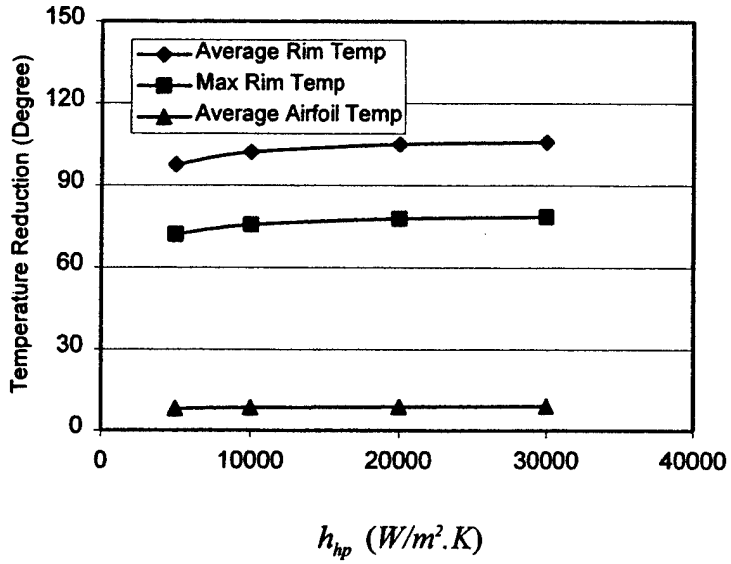

Fig. 5.9 Average and maximum temperature reductions at the disk rim and average temperature reduction at the airfoil surface with the different effective thermal conductance of heat pipes (d_{hp}=0.008 m, T_c = 798 K, L_{hp}=0.1 m).

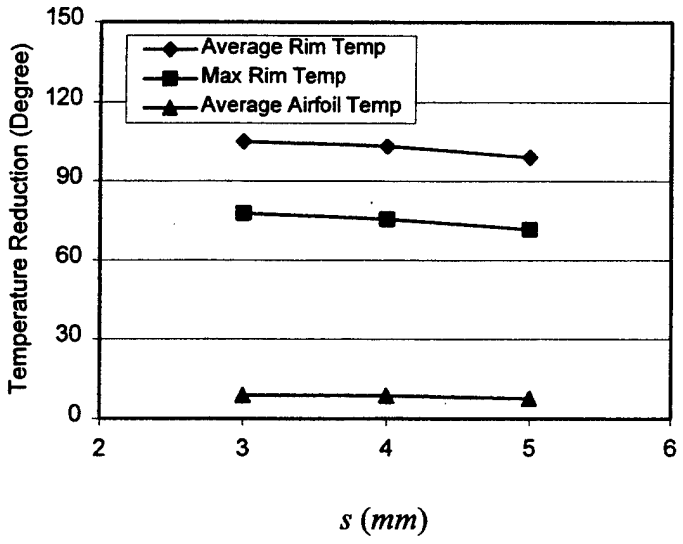

Fig. 5.10 Average and maximum temperature reductions at the disk rim and average temperature reduction at the airfoil surface with different s (d_{hp}=0.008 m, h_{hp}=20,000 $W/m^2.K$, L_{hp}=0.1 m).

References

Arpaci, V. S., 1966, *Conduction Heat Transfer*, Addison-Wesley Publishing Company, Menlo, California.

Cao, Y., 1997, "A Feasibility Study of Turbine Disk Cooling by Employing Radially Rotating Heat Pipes," *Final Report for Summer Faculty Research Program (Wright Laboratory)*, sponsored by Air Force Office of Scientific Research and Turbine Engine Division, Wright Laboratory.

Cao, Y. and Chang, W.S., 1997, "Analyses of Heat Transfer Limitations of Radially Rotating Heat Pipes for Turbomachinery Applications," AIAA 97-2542, *32nd Thermophysics Conference*, Atlanta, GA.

Cao, Y., Gao, M.C., Beam, J.E., and Donovan, B., 1997, "Experiments and Analyses of Flat Miniature Heat Pipes," *AIAA Journal of Thermophysics and Heat Transfer*, Vol. 11, No. 2, pp. 158 – 164.

Cao, Y., Chang, W.S. and MacArthur, C., 1998, "An Analytical Study of Turbine Disks Incorporating Radially Rotating Heat Pipes," ASME IMECE, Anaheim, CA.

Cao, Y., Ling, J., Rivir, R. and MacArthur, C., 2000, "A Numerical Analysis of Gas Turbine Disks Incorporating Rotating Heat Pipes," ASME *IMECE*, Vol. 3, pp. 61-67, Orlando, Florida.

Dunn, P.D. and Reay, D.A., 1994, *Heat Pipes*, Fourth Edition, Pergamon.

Jian Ling and Yiding Cao, 2000, "Closed-Form Analytical Solutions for the Radially Rotating Miniature High-Temperature Heat Pipes Including Non-Condensable Gas Effects," International J. of Heat and Mass Transfer, Vol. 43, No. 19, pp. 3661-3671.

Jian Ling, Yiding Cao and W. S. Chang, 1999, "Analysis of Radially Rotating High-Temperature Heat Pipes for Turbomachinery Application, " *ASME,* Journal of engineering for Gas Turbines and Power, Vol. 121, pp. 306-312.

Metzger, D.E., Mathis, W.J., and Grochowsky, L.D., 1979, "Jet Cooling at the Rim of a Rotating Disk," *Journal of Engineering for Power*, Vol. 101, pp. 68-72.

Metzger, D.E. and Grochowsky, L.D., 1977, "Heat Transfer Between an Impinging Jet and a Rotating Disk," *ASME Journal of Heat Transfer*, Vol. 99, No. 4.

Metzger, D. E., 1970, "Heat Transfer and Pumping on a Rotating Disk With Freely Induced and Forced Cooling," *Journal of Engineering for Power*, July, 1970, pp. 342-348.

Ozisik, M. N., 1993, *Heat Conduction*, 2nd Edition, John Wiley & Sons, Inc., New York, Chichester.

Owen, J..M., 1988, "Air-Cooled Gas-Turbine Discs: a Review of Recent Research," *Int. J. Heat and Fluid Flow*, Vol. 9, No. 4, pp. 354-365.

Owen, J.M., 1992, "Recent Developments in Rotating-Disc Systems," *ImechE*, pp. 83-92.

Ponnappan, R., He, Q., and Leland, J.E., 1997, "Test Results of a High Speed Rotating Heat Pipe," AIAA 97-2543.

Schreiber, R., 1992, "Assessing Holemaking Alternatives," *Manufacturing Engineering*, May, 1992, pp. 37-41.

Shepherd, D.G., 1972, Aerospace Propulsion, American Esevier Publishing, New York, London.

LIST OF SYMBOLS

C_1, C_2 and C_3 constants in section 4

$C_{1\varepsilon}$, $C_{2\varepsilon}$ and C_μ constants in the turbulent model of section 5

C_p specific heat at constant pressure, J/kg-K

d, d_{hp} heat pipe diameter, m

d_i heat pipe inner diameter, m

d_o heat pipe outer diameter, m

E empirical constant

g acceleration of gravity, m/s^2

h heat transfer coefficient, W/m^2-K, or specific enthalpy, kJ/kg

I, K modified Bessel functions of the first and second kinds

k thermal conductivity or turbulent kinetic energy, W/m-K or m^2/s^2

k_v von Karman's constant

k_a average or effective thermal conductivity of the disk, W/m-°C

k_{eff} effective thermal conductance of heat pipe, W/m-°C

L half disk thickness or heat pipe length, m

L_{hp} heat pipe length, m

Q heat transfer rate, W

q'' heat flux, W/cm^2

q''_{rad} radiation heat flux, W/cm^2

r radial position, m

r_1, r_2 inner and outer radii of the disk, m

r_{hp} heat pipe radius, m

s distance between the disk rim and heat pipe top, m

Δs distance, m

t time, s

T temperature, K

T_c, T_{air} cooling air temperature, K

u velocity component, m/s

W flow rate of cooling air, m^3/s, in section 2, and disk wall surface in section 3, m

x, y, z coordinate systems

$\overline{Z}_a$ average revolving radius of the heat pipe, m

Greek Symbols

ρ density, kg/m^3

η_m eigenvalues

ω angular velocity

θ temperature difference, $\theta = T-T_c$, degree

θ_{max} maximum temperature difference, $\theta_{max} = T_{max}-T_c$, degree

ε dissipation rate of turbulent kinetic energy, m^2/s^3

μ dynamic viscosity, $N-s/m^2$

Subscripts

hp heat pipe

air, gas cooling air or gas

i, j, k general spatial indices